COMBINED STUDIES

TEXAS INSTRUMENTS,
INCORPORATED, DALLAS

31 AUGUST 1976

ALEX(02)-FR-76-01

COMBINED STUDIES

FINAL REPORT

23 APRIL 1973 TO 31 AUGUST 1976

Prepared by
Lawrence S. Turnbull, Jr. and David Sun

TEXAS INSTRUMENTS INCORPORATED
Equipment Group
Post Office Box 6015
Dallas, Texas 75222

Contract No. F44620-73-C-0055
Amount of Contract: $294,749
Beginning 23 April 1976
Ending 30 June 1976

Prepared for

AIR FORCE OFFICE OF SCIENTIFIC RESEARCH

Sponsored by

ADVANCED RESEARCH PROJECTS AGENCY
Nuclear Monitoring Research Office
ARPA Program Code No. F10
ARPA Order No. 1827

31 August 1976

Acknowledgment: This research was supported by the Advanced Research Projects Agency, Nuclear Monitoring Research Office, under Project VELA-UNIFORM, and accomplished under the direction of the Air Force Office of Scientific Research under Contract Number F44620-73-C-0055.

COMBINED STUDIES

FINAL REPORT

23 APRIL 1973 TO 31 AUGUST 1976

Prepared by
Lawrence S. Turnbull, Jr. and David Sun

TEXAS INSTRUMENTS INCORPORATED
Equipment Group
Post Office Box 6015
Dallas, Texas 75222

Contract No. F44620-73-C-0055
Amount of Contract: $294,749
Beginning 23 April 1976
Ending 30 June 1976

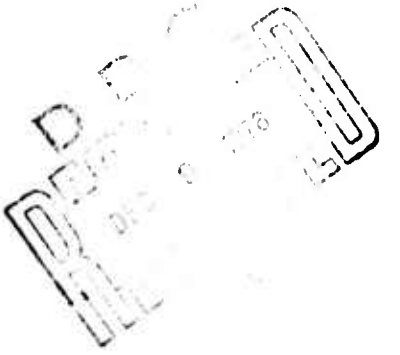

Prepared for

AIR FORCE OFFICE OF SCIENTIFIC RESEARCH

Sponsored by

ADVANCED RESEARCH PROJECTS AGENCY
Nuclear Monitoring Research Office
ARPA Program Code No. F10
ARPA Order No. 1827

31 August 1976

Acknowledgment: This research was supported by the Advanced Research Projects Agency, Nuclear Monitoring Research Office, under Project VELA-UNIFORM, and accomplished under the direction of the Air Force Office of Scientific Research under Contract Number F44620-73-C-0055.

REPORT DOCUMENTATION PAGE

READ INSTRUCTIONS BEFORE COMPLETING FORM

1. REPORT NUMBER AFOSR - TR - 76 - 1262	2. GOVT ACCESSION NO. / 3. RECIPIENT'S CATALOG NUMBER
4. TITLE (and Subtitle) COMBINED STUDIES FINAL REPORT	5. TYPE OF REPORT & PERIOD COVERED Final 04/23/73 to 08/31/76
	6. PERFORMING ORG. REPORT NUMBER ALEX(02)-FR-76-01
7. AUTHOR(s) Lawrence S. Turnbu , Jr., and David Sun	8. CONTRACT OR GRANT NUMBER(s) F44620-73-C-0055
9. PERFORMING ORGANIZATION NAME AND ADDRESS Texas Instruments Incorporated Equipment Group Dallas, Texas 75222	10. PROGRAM ELEMENT, PROJECT, TASK AREA & WORK UNIT NUMBERS ARPA Program Code No. F10
11. CONTROLLING OFFICE NAME AND ADDRESS Advanced Research Projects Agency Nuclear Monitoring Research Office Arlington, Virginia 22209	12. REPORT DATE 31 August 1976 13. NUMBER OF PAGES 64
14. MONITORING AGENCY NAME & ADDRESS(if different from Controlling Office) Air Force Office of Scientific Research Bolling Air Force Base, Bldg. 410 Washington, D.C. 20332	15. SECURITY CLASS. (of this report) UNCLASSIFIED 15a. DECLASSIFICATION DOWNGRADING SCHEDULE

16. DISTRIBUTION STATEMENT (of this Report)

APPROVED FOR PUBLIC RELEASE, DISTRIBUTION UNLIMITED

17. DISTRIBUTION STATEMENT (of the abstract entered in Block 20, if different from Report)

18. SUPPLEMENTARY NOTES

ARPA Order No. 1827

19. KEY WORDS (Continue on reverse side if necessary and identify by block number)

Seismology
Surface Waves
Spectral Fit
Counterevasion
Complex Cepstrum
Eigenspectrum Analysis

20. ABSTRACT (Continue on reverse side if necessary and identify by block number)

Work performed on the combined studies contract (F44620-73-C-0055), which included the evaluation of counterevasion techniques and the use of far-field seismic data to determine attenuation and source parameters, has been discussed in detail in six semi-annual technical reports, technical memoranda, and a doctoral dissertation. This final report summarizes the material covered in those items and discusses the conclusions obtained from these studies. The counterevasion studies were

20. continued

concerned with the evaluation and application of two techniques, complex cepstrum analysis and eigenspectrum analysis. These techniques were used to separate interfering seismic signals in order to distinguish underground nuclear explosions hidden in larger earthquakes, for the identification of sequential underground nuclear explosions, and for the detection of the pP depth phase. In addition, a new study on the effect of sampling rate on the detection of the pP depth phase is also presented.

The main topic of the far-field research was directed toward the determination of seismic source parameters using teleseismic surface wave spectra. Techniques were developed to fit theoretical spectra generated using a double couple source in a layered half-space to observed spectra corrected to a near source reference point. Several procedures were used to correct the observed spectra for effective attenuation. As a result, effective attenuation values were obtained for many Eurasian and North American travel paths. Finally, the far-field studies also included a comparative analysis of upper mantle Q and other geophysical data on the Eurasian continent.

ABSTRACT

Work performed on the combined studies contract (F44620-73-C-0055), which included the evaluation of counterevasion techniques and the use of far-field seismic data to determine attenuation and source parameters, has been discussed in detail in six semiannual technical reports, technical memoranda, and a doctoral dissertation. This final report summarizes the material covered in those items and discusses the conclusions obtained from these studies. The counterevasion studies were concerned with the evaluation and application of two techniques: complex cepstrum analysis and eigenspectrum analysis. These techniques were used to separate interfering seismic signals in order to distinguish underground nuclear explosions hidden in larger earthquakes, for the identification of sequential underground nuclear explosions, and for the detection of the pP depth phase. In addition, a new study on the effect of sampling rate on the detection of the pP depth phase is also presented.

The main topic of the far-field research was directed toward the determination of seismic source parameters using teleseismic surface wave spectra. Techniques were developed to fit theoretical spectra generated using a double couple source in a layered half-space to observed spectra corrected to a near source reference point. Several procedures were used to correct the observed spectra for effective attenuation. As a result, effective attenuation values were obtained for many Eurasian and North American travel paths. Finally, the far-field studies also included a comparative analysis of upper mantle Q and other geophysical data on the Eurasian continent.

TABLE OF CONTENTS

LIST OF FIGURES

LIST OF FIGURES
(continued)

SECTION I
COUNTEREVASION STUDIES

A. INTRODUCTION

For the past three years, we have evaluated and applied two methods to separate interfering seismic signals: cepstrum analysis and eigenspectrum analysis. These techniques have potential value for counterevasion studies in that they are expected to achieve these three goals: to distinguish underground nuclear explosions hidden in larger earthquakes; to identify sequential underground nuclear explosions disguised as earthquakes; and to detect the pP depth phase for the estimation of the burial depth of the underground nuclear explosion. In this report, we present a brief summary of work given in previous technical reports and a study on the effect of the sampling rate to the detection of the pP phase by the cepstrum analysis.

Work on the counterevasion studies that has already been reported is summarized in Subsection B. The mathematical description underlying these two methods is briefly reviewed, and the experimental results obtained at various stages are discussed. In Subsection C, the results from the study on the effect of the sampling rate are discussed. This study concludes the continuing effort in searching for the favorable factors to help the cepstrum analysis to achieve better results in detecting the pP phase.

B. SUMMARY OF PREVIOUS WORK

The cepstrum analysis and the eigenspectrum analysis have been applied to markedly different combinations of interfering seismic signals for quite different purposes. The cepstrum analysis separates signals from

the same azimuth, the waveforms and thus spectra of which are similar. The eigenspectrum analysis, by contrast, is used to separate signals from different azimuths, with greatly different spectra; it considers the data over a narrow frequency band. Hence, the work involved in the evaluation and application of these two methods has been handled and reported as two independent tasks for the whole contract period. Consequently, in the following sections, the summary of previous work will be given separately for these two analyses.

1. Eigenspectrum Analysis

The theoretical basis for the eigenspectrum analysis was discussed in Semiannual Technical Report No. 1, as were some details of the method of calculation and errors which might be expected. The ability of the eigenspectrum analysis to separate the off-azimuthal interfering signals lies in the identification of the eigenvalues of the data matrix with the signal powers and the eigenvectors with the signal vectors. In the eigenspectrum analysis, the data matrix is formed and its eigenvalues and eigenvectors are computed. The data matrix Ω is formed as follows:

$$\Omega = SS^H, \tag{I-1}$$

where H stands for conjugate transpose, and S is the total signal vector recorded at an array of sensors, defined by:

$$S = [\ldots F_i(f) \ldots]^T$$

where T denotes transpose and $F_i(f)$ is the amplitude spectrum at frequency f for the ith site. There are N eigenvalues of the data matrix Ω, where N is the number of sites in the array, and they are S^HS, O, O.... The associated eigenvector is V for the non-zero eigenvalue.

If only one signal, of wavenumber vector k, is presented at the array, we have tne following:

$$S^H S/N = V^H V/N = \text{signal power at a site,}$$

and the eigenvector V is in the direction of wavenumber vector k. However, when two signals, S_1 and S_2, are present, the data matrix Ω defined by equation (I-1) at a single frequency contains the cross-correlation terms, $S_1 S_2^H$ and $S_2 S_1^H$, as follows:

$$\Omega = S_1 S_1^H + S_2 S_2^H + S_1 S_2^H + S_2 S_1^H. \qquad \text{(I-2)}$$

The existence of these two cross-correlation terms makes the eigenspectrum analysis useless for its purpose. To eliminate them, the data matrix Ω is averaged over a finite band of frequencies. Under the assumption that signals are uncorrelated, the average data matrix becomes:

$$\bar{\Omega} = \overline{S_1 S_1^H} + \overline{S_2 S_2^H}. \qquad \text{(I-3)}$$

However, in doing so, the interpretation of the eigenvalues of the average data matrix $\bar{\Omega}$ as the average signal power, in general, is lost. Thus, in practice, we average the data matrix Ω over a frequency band wide enough to eliminate most of the cross-correlation terms, yet narrow enough not to change the eigenvalues too much from the average signal powers.

In Semiannual Technical Report No. 1, the eigenspectrum analysis was applied to the synthetic signals formed from the chirp sinusoidal waveforms, which exhibited dispersion and simple amplitude modulation. The data matrix was constructed from these waveforms, which were identical at each site except for time shifts appropriate to the sites of a hypothetical seven element hexagonal array of 50 km diameter, similar to the inner ring of sensors at ALPA. The major results can be summarized as follows:

- The eigenspectrum analysis has marked superiority over both the beamsteering and maximum likelihood methods in its ability to find small signals in the presence of large ones, for signal models based on chirp waveforms.

- Over a wide azimuthal range, the eigenspectrum analysis can resolve signals down to 27 dB below another interfering signal.

- The presence of noise did not interfere with the extraction of one signal from the other, unless the noise was as large as the smaller signal.

With the success in applying the eigenspectrum analysis to the synthetic signals formed from the chirp sinusoidal waveforms, the real seismic signals recorded at sites 1 through 16 of ALPA were employed next, and the results were presented in Semiannual Technical Report No. 2. To form the interfering events, Fourier transforms of appropriate signals were added, site by site. The data matrix was constructed from these summed transforms, so that all appropriate cross-correlation terms were present to simulate the real interfering events.

The experimental work with these real signals indicates the following conclusions:

- The eigenspectrum analysis is capable of closely estimating the power and azimuth of a signal 20 dB below another interfering signal.

- Care must be taken to choose the proper frequency band over which to observe them. When this is done, noise due to the seismic source and to the calculation sets the low limit on the resolution power of the technique.

These conclusions were drawn from the experimental results on a particular calculation involving the mixture of two specific real signals. Further research showed that such results were the exception rather than the rule. The results obtained from the further study on the effects of averaging the data matrix over a frequency to the eigenspectrum analysis were reported in Semiannual Technical Report No. 3. These results illustrated the difficulties encountered and suggested their origin. These problems are inherent in the use of real data and appear to make eigenspectrum analysis inapplicable in the general case. The conclusions reached by this study are as follows:

- The averaging process does not result in completely uncorrelated data matrices corresponding to the first and the second signals. Some non-negligible cross-correlation terms between the signals are still presented after the averaging process. These terms reflect the fact that signals of finite length are in general correlated. Their effect at small differences in power between the first and the second signals is to distort the second eigenvalue significantly from its correct value. Nevertheless, the direction of the second eigenvector is not affected.

- At larger power separations between the two signals, another effect appears: there is always a spurious component in the second eigenspectrum due to the effect of averaging the signal vector of the larger signal over frequency. This component interferes with that due to the second signal when the second signal power is at or below the power of the spurious component, resulting in the incorrect estimation of the azimuth as well as the power of the second signal in this case.

- The effects of frequency averaging can be eliminated by constructing the data matrix in appropriate, yet unrealistic, ways, which allow resolution of small signals at power separations

down to 50 dB. However, it is not possible to find the data matrices in these ways for real interfering signals as recorded, so that the problems encountered here generally appear insurmountable. The eigenspectrum analysis, then, as presently implemented, is unable to resolve interfering signals at any useful range of power separations.

In the hope of replacing eigenspectrum analysis -- which we showed to be inapplicable to real seismic signals -- we have proposed and examined a time-domain signal stripping technique. Work performed was reported in Technical Memorandum dated February 27, 1976, by David Sun. The proposed time-domain signal stripping was found to be a special case of the iterative beamforming technique, which was developed, evaluated, and recently reported by Blandford et al. (1975). To avoid repetition of this effort, no further work was carried out on this technique.

2. Cepstrum Analysis

The conceptual formulation and general mathematical description of the cepstrum analysis were discussed in great detail by Schafer (1969). Several detailed mathematical expressions of the complex cepstrum for our specific applications of the cepstrum analysis were derived and discussed in various semiannual technical reports.

The complex cepstrum $\hat{s}(n)$ of the sampled time function $s(n)$ can be obtained from this general set of equations:

$$S(z) = \sum_n s(n)\, z^{-n}$$

$$\hat{S}(z) = \ell n \{S(z)\}$$

$$\hat{s}(n) = \frac{1}{2\pi j} \oint \hat{S}(z)\, z^{n-1}\, dz, \qquad \text{(I-4)}$$

where

$S(z)$ = the z-transform of $s(n)$,

$\oint$ = a contour integral about zero, and

j = $\sqrt{-1}$.

Let us consider a mixed signal consisting of two identical signals as follows:

$$X(n) = s(n) + as(n - n_o) \quad , \tag{I-5}$$

or equivalently in the convolution form as follows:

$$x(n) = s(n) * m(n) \quad , \tag{I-6}$$

where

$m(n)$ = $\delta(n) + a\delta(n - n_o)$ ($\delta(n)$ is the Dirac delta function) is the multipath operator which convolves with the signal,

n_o = the time delay, and

a = a scale constant (for convenience, yet without loss of generality, les us assume ($|a| < 1$)).

The complex cepstrum $\hat{x}(n)$ of $x(n)$ will be as follows:

$$\hat{x}(n) = \hat{s}(n) + \hat{m}(n) \quad , \tag{I-7}$$

where $\hat{s}(n)$ and $\hat{m}(n)$ are complex cepstra of $s(n)$ and $m(n)$ respectively, and

$$\hat{m}(n) = \sum_{k=1} (-1)^{k+1} \frac{a^k}{k} \delta(n - kn_o) \quad . \tag{I-8}$$

In general, $\hat{s}(n)$ and $\hat{m}(n)$ are separable in the sense that large terms of $\hat{s}(n)$ occur at shorter time than do the large terms of $\hat{m}(n)$. Hence, $s(n)$ can be recovered by shortpass filtering $\hat{x}(n)$ and by taking the inverse process of the transformation given by equation (I-4). By recovering

$s(n)$, the delay time n_o, and the relative amplitude of the two arrivals -- i.e., a -- can be easily estimated. Estimation of the delay times and relative amplitudes of the later arrivals in a given mixed signal has been the main purpose of using the cepstrum analysis is the counterevasion study.

Now when there is additive noise $\epsilon(n)$, i.e.,

$$x(n) = s(n) + a\,s(n - n_o) + \epsilon(n) \quad , \tag{I-9}$$

the complex cepstrum $x(n)$ will become:

$$\hat{x}(n) = \hat{s}(n) + \hat{m}(n) + z\text{-transform}^{-1}\left[\ell n\left(1 + \frac{E(z)/S(z)}{1 + a\,z^{-n_o}}\right)\right] \tag{I-10}$$

where $E(z)$ is the z-transform of $\epsilon(n)$, and z-transform$^{-1}[\ ]$ stands for inverse z-transform. The recovered signal $\underset{\sim}{s}(n)$ by the cepstrum analysis will be as follows:

$$\underset{\sim}{s}(n) = s(n) + z\text{-transform}^{-1}\left[\frac{E(z)}{1 + a\,z^{-n_o}}\right] \quad . \tag{I-11}$$

Equations (I-10) and (I-11) show how the noise will affect the cepstrum analysis on the detection of the cepstral peaks due to the second arrival and on the estimation of the delay time n_o and the signal $s(n)$.

The above derivations are based on the assumption that the later arrival is the exact replica of the first arrival, which, of course, will not be observed in real seismic signals. When two arrivals are non-identical, i.e.,

$$x(n) = s_1(n) + s_2(n - n_o) \quad , \tag{I-12}$$

the complex cepstrum can be represented as follows:

$$\hat{x}(n) = \hat{s}_1(n) + \hat{m}(n) + z\text{-transform}^{-1}\left[\ell n\left(1 + \frac{Ed(z)\, z^{-n_o}/S_1(z)}{1 + a z^{-n_o}}\right)\right] . \qquad \text{(I-13)}$$

The resolved signal $\underset{\sim}{s}_1(n)$ by the cepstrum analysis will be as follows:

$$\underset{\sim}{s}_1(n) = s_1(n) + z\text{-transform}^{-1}\left[\frac{Ed(z)\, z^{-n_o}}{1 + a z^{-n_o}}\right] . \qquad \text{(I-14)}$$

In equations (I-1) and (I-14), $Ed(z)$ is the z-transform of $\epsilon d = s_2(n) - a s_1(n)$. Equations (I-13) and (I-14) will be a good representation when $s_1(n)$ and $s_2(n)$ are similar. Good similarity between two arrivals can be expected in the real seismic signals, such as the P-phase and its pP-phase.

The cepstrum analysis was first applied to synthetically-mixed signals consisting of two identical arrivals, which were the short period P-waves of presumed underground explosions from the eastern Kazakh (EKZ) recorded at NORSAR. Results were discussed in Semiannual Technical Report No. 1. Results were quite satisfactory and encouraging; they validated the basic software implementing the cepstrum analysis and numerically confirmed the capability of the cepstrum analysis in decomposition of a mixed signal consisting of two identical signals.

Next, the synthetically-mixed signals were formed from two or three non-identical arrivals. Again, the short period P-waves of presumed underground nuclear explosions from EKZ as recorded at NORSAR were used. The delay time and the relative amplitude of the second arrival with respect to the first arrival were varied within some realistic ranges. The detailed discussion of the results was presented in Semiannual Technical Report No. 2. The major results of this study are as follows:

- Using cepstrum analysis, the short period seismic P-waves, composed of at least three separate events, are separable into

their component events, when these events were separated by arrival time by times not less than n_{min}. This n_{min} varies between 0.5 and 0.7 seconds and varies for different events.

- This minimum delay time, n_{min}, appears to be predetermined by the P-pP delay time of the first event used in forming the mixed signal.

- The relative amplitude of the second arrival with respect to the first arrival is not too critical to the successful cepstrum analysis. The maximum relative amplitude is determined by the machine accuracy in the unweighting process of the cepstrum analysis.

Using the synthetically-mixed signals, the cepstrum analysis was proved to be able to decompose a mixed signal into its constituent arrivals. Also, it was realized that the short period P-waves of presumed underground nuclear explosions, which were used to form the synthetically-mixed signals, usually contained more than a single phase. In most cases, they were composed of a direct P-phase and a surface reflected pP-phase. Hence, in Semiannual Technical Report No. 3, the cepstrum analysis was applied to several short period P-waves of presumed underground nuclear explosions from the EKZ as recorded at NORSAR. This application serves to purposes: First, to determine whether the cepstrum analysis can be applied to the real seismic signals and whether the P-pP delay time estimated by the cepstrum analysis agrees with those calculated by some other means; and, second, using the cepstrum resolved P-phase and pP-phase to find the minimum P-pP delay time that the cepstrum analysis can still work successfully. The major results are as follows:

- The cepstrum analysis can successfully resolve the depth phases (pP) from the P-waves of presumed underground nuclear explosions. The P-pP delay times estimated by the

cepstrum analysis agree very well with those calculated by the cube-root scaling law which estimates the burial depth of a contained explosion from the bodywave magnitude (m_b) and the yield.

- The estimated P-pP delay times range from 0.4 to 0.9 second for the presumed EKZ explosions with an m_b ranging from 4.9 to 6.0.

- The complex cepstra of the resolved P-phases of the presumed EKZ explosions are concentrated within 0.4 to 0.6 second around the zero cepstrum time. This makes the shortpass filter work satisfactorily only for the P-pP delay time greater than 0.4 second. For shorter delay times, the combination of the comb and the shortpass filter can be used. However, in order to use the comb filter, the P-pP delay time and the amplitude ratio of the pP-phase to the P-phase have to be estimated before filtering.

Further application of the cepstrum analysis to the real seismic signals led to the analysis of a number of presumed underground nuclear explosions in Eurasia assumed to be for some peaceful use. All such events occurring through 1973 for which good array data were available were examined. Fifteen events were recorded with good signal-to-noise ratio at LASA. Three of these events were far enough from NORSAR to provide usable teleseismic records there. Results were discussed in Semiannual Technical Report No. 4 and are reiterated below:

- Cepstrum analysis can recover depth phases from real underground nuclear explosions in regions of complicated geology. The estimates of the P-pP delay times of these events are consistent with all the events being contained.

- Cepstrum analysis is believed to be able to resolve possible multiple arrivals in the real teleseismic short period P-waves of presumed explosions. However, the resolved multiple arrivals may come from a real multiple explosion or may be attributed to the non-source oriented effects, such as surface reverberations.

- Where the depth phase can be identified, its delay time can be determined well within the accuracy required for discrimination.

- The cepstrum-resolved depth phase amplitude may be larger than the theoretically-expected value by a factor of two. This may be caused by the surface focusing or directional propagation.

After successful application of the cepstrum analysis to both synthetically-mixed and real seismic signals, we looked into those factors which might be unfavorable or favorable to the cepstrum analysis in its performance, especially in the detection of the P-pP delay time and in the successful decomposition of the P-wave into the P-phase and the pP-phase. The effects of the unfavorable factors -- specifically, the noise, the dissimilarity between the P-phase and the pP-phase, and the prefiltering -- were studied and discussed in Semiannual Technical Report No. 5 and are presented below:

- The dissimilarity will affect the detection more seriously than the noise. The increase of the noise level will only gradually obscure the cepstral peaks due to the P-pP delay time, while the dissimilarity completely destroys the periodic occurrences of these cepstral peaks. For the identical P-phase and the pP-phase, the cepstrum analysis can detect the P-pP delay time as short as 0.4 second and can successfully recover them for the signal-to-noise ratio as low as 12 dB. For the

non-identical P-phase and pP-phase, the cepstrum analysis can still achieve the successful decomposition for the similarity coefficient about 0.55. This, in turn, can be used to estimate the P-pP delay time.

- In reality, the pP-phase and the P-phase are not identical, although they can be expected to be quite similar. Therefore, for the real seismic P-waves, we should not expect to find the periodicity of the cepstral peaks due to the P-pP delay time. Rather, we should look for the suspicious cepstral peaks and filter the cepstrum accordingly for the possible decomposition. The correct estimate of the P-pP delay time can be obtained only through the successful cepstrum decomposition of the mixed signal.

- Prefiltering, in general, does not affect the cepstrum-analyzed results as long as the passband of the filter covers the entire signal spectrum. The reduction of the noise by prefiltering does not compensate for the effect of minor distortion of the amplitude spectrum (associated with the prefiltering on the detection of the P-pP delay time). Consequently, it is suggested that the prefiltering should be avoided if the signal-to-noise ratio is not unreasonably low.

Knowing the effects of those unfavorable factors to the cepstrum analysis, we studied several possible means to combat them, specifically beamforming and sampling. Beamforming in the cepstrum time domain (BFCEP) was discussed in Semiannual Technical Report No. 6, and the effect of the sampling rate will be discussed in the next subsection. Moreover, the capability of the cepstrum analysis was further evaluated and validated by undertaking the following two tasks:

- Analysis of fifteen earthquakes with known PDE depths.
- Analysis of two presumed underground nuclear explosions from the EKZ using P-waves recorded at several different NORSAR subarrays.

Results from these two analyses were also discussed in Semiannual Technical Report No. 6 and are summarized as follows:

- Among the fifteen earthquakes being analyzed, the percentage of possible misdecompositions by cepstrum analysis is low, about 10% at the worst. While the misdecomposition may be caused by the inherent defect of the complex cepstrum technique, it is more likely that misdecomposition is caused by lack of more restricted criteria for analyzing earthquake signals.
- Cepstrum-resolved delay times, especially the P-pP delay times, can be expected to be quite reliable, even when only one recorded signal is used. However, the amplitude ratios among the resolved signals vary quite noticeably among several signals recorded at different stations. The idea of cepstrum analysis of an event with signals recorded at several different stations is good in the sense that several independent estimates for the same event can be obtained, and results common to these estimates can then be taken to be the source effect with more confidence.
- Beamforming in the cepstrum time domain is proved to be effective in improving the detection of the cepstral peaks due to the P-pP delay time. In general, the BFCEP achieves its goal through the reduction of the cepstral level of the surrounding cepstra.

- For the high signal-to-noise ratio (SNR) -- above 18 dB -- the BFCEP is not necessary, because the beamed cepstrum and the cepstrum of the individual channel are practically the same. However, for the low SNR -- below 12 dB -- the BFCEP can give significant improvement in the detection. The beamed cepstra for the SNR of 12 dB and 6 dB are almost identical to that for the SNR of 18 dB, and all give equally fair detection.

- For the multiple arrivals which are not the source effect, the BFCEP does improve the detection noticeably. The maximum reduction in the cepstral level of the surrounding cepstra is $\frac{1}{N}$, where N is the number of channels used in the BFCEP.

- For the dissimilarity of the P-phase and the pP-phase, the BFCEP can improve the detection by sharpening the first suspicious cepstral peak and by reducing significantly the cepstral level of the surrounding cepstra. However, the BFCEP has not brought back the periodicity of the cepstral peaks, as indicated by equation (I-13). This equation will give an even easier and firmer detection.

C. EFFECT OF SAMPLING RATE ON THE DETECTION OF THE P-pP DELAY TIME

1. Introduction

In our previous work, cepstrum analysis was applied to the short period P-waves which were sampled at the rate of 10 samples per second (samples/sec). There are several obvious reasons for using a sampling rate of 10 samples/sec. First, 10 samples/sec is the sampling rate of the recorded short period signals which are available to us. Second, this sampling rate is already above the Nyquist rate for most of the short period P-waves of presumed underground nuclear explosions. Third, to avoid introducing the high frequency noise into the complex cepstrum, sampling at a rate equal to or just a little bit greater than the Nyquist rate has been suggested for numerical computation (Schafer, 1969; Lane and Sun, 1974a).

To illustrate the last point above, Figure I-1 shows the amplitude spectra of three sampled short period signals which are obtained from the same short period P-wave by sampling at three different rates: 10 samples/sec, 20 samples/sec, and 40 samples/sec. It is noticed that the energy of this signal is well confined below 5 Hz. Hence, the sampling rate of 10 samples/sec is very close to the Nyquist rate for this signal. Therefore, oversampling at 20 and 40 samples/sec gains no extra information about the signal spectrum, except that it introduces some high frequency noise beyond the Nyquist frequency due to the inaccuracy of numerical computation. This high frequency noise present there is transformed into the cepstrum time domain as noise. This seems to imply that oversampling a signal will only make its complex cepstrum noisier. However, giving it some more thought, it appears that oversampling might help the cepstrum analysis on the detection and estimation of the P-pP delay time with the noisier complex cepstrum as the tradeoff. In the following paragraphs, we will first discuss how and why

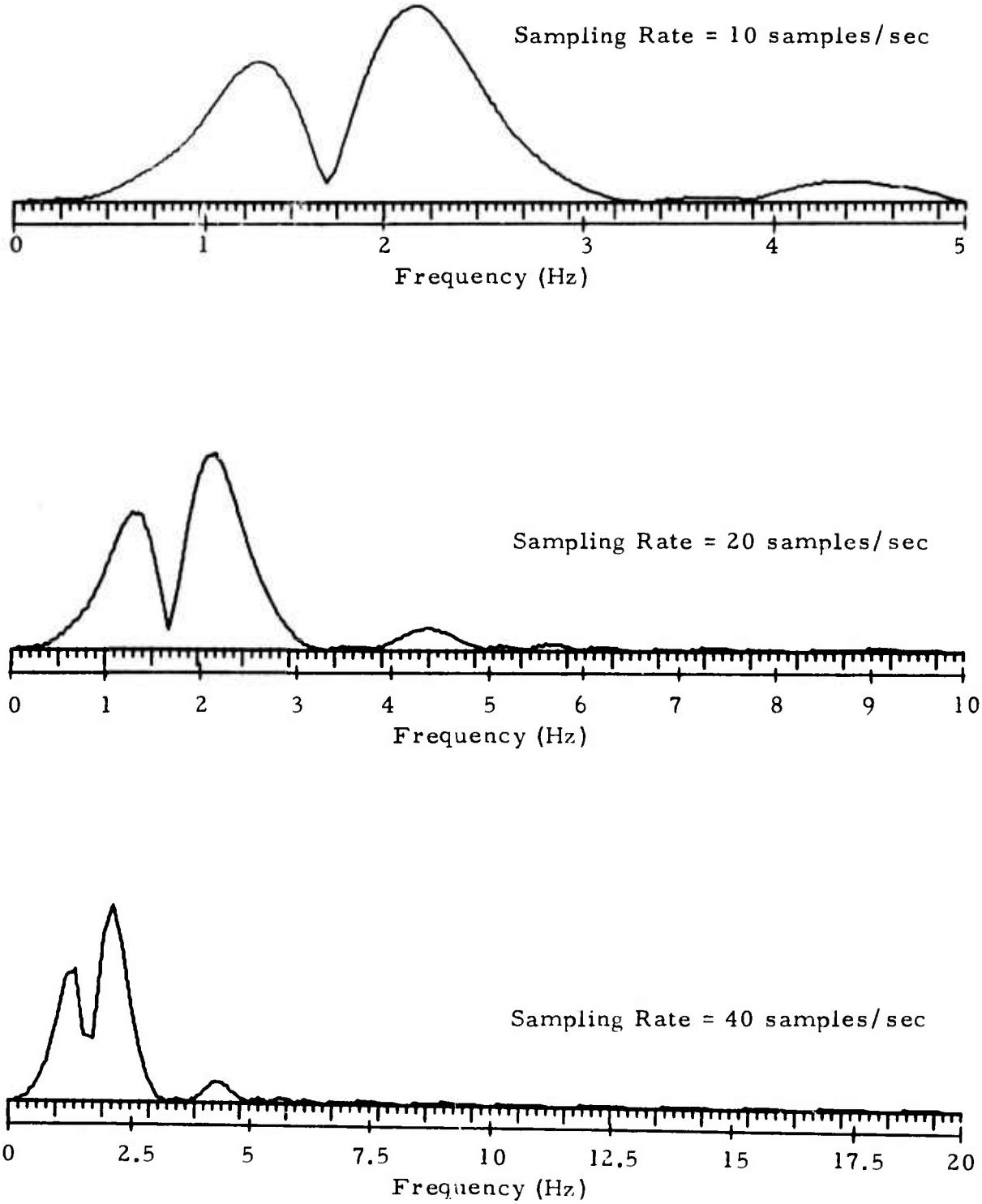

FIGURE I-1

AMPLITUDE SPECTRUM OF A SIGNAL FOR THREE DIFFERENT SAMPLING RATES

the sampling rate can affect the detection of the P-pP delay time. Then, the results from applying cepstrum analysis to mixed signals of various sampling rates will be presented.

2. Qualitative Discussion

Let us consider a mixed signal consisting of two identical signals, which may simulate the P-phase and the pP-phase, as follows:

$$x(t) = s(t) - a\,s(t - t_o), \tag{I-15}$$

where a is a scale constant and t_o is the delay time in seconds. The signal $x(t)$ sampled at the rate of $\frac{1}{\Delta t}$ will be as follows:

$$x(n) = s(n) - a\,s(n - n_o). \tag{I-16}$$

It is clear that $n_o \Delta t$ will be exactly equal to t_o second if and only if $x(t)$ is sampled at a rate such that $t_o/\Delta t$ is an integer. Thus, higher sampling rate, i.e., smaller Δt, will make $n_o \Delta t$ a better approximation of t_o. Therefore, intuitively, we will expect that cepstrum analysis should yield a better estimation of t_o from n_o by using signals sampled at a higher rate. The complex cepstrum of $x(n)$ will be as follows:

$$\hat{x} = \hat{s}(n) - \hat{m}(n) \tag{I-17}$$

with

$$\hat{m}(n) = \sum_{k=1} \frac{a^k}{k}\, \delta(n - kn_o).$$

The capability of the cepstrum analysis in estimating t_o relies heavily on the visual identification of the first few cepstral peaks of $\hat{m}(n)$. How well these cepstral peaks can be identified depends on how clear they can be distinguished from the surrounding cepstra, i.e., $\hat{s}(n)$. From equation (I-17), it is clear

that within the same duration of cepstrum time, say, $0 < t < T$, the number of the cepstral peaks of $\hat{m}(n)$ is a constant which depends on t_o and is independent of the sampling rate. However, the number of samples of $\hat{s}(n)$ within that same cepstrum time will be proportional to the sampling rate. Therefore, it is conjectured that the first few cepstral peaks of $\hat{m}(n)$ might stand out better from the surrounding cepstra $\hat{s}(n)$ for higher sampling rate if the cepstrum noise introduced by oversampling remains well below the cepstral level of $\hat{m}(n)$. This can be better explained by considering a very short delay time, say, $t_o = 0.1$ second. For a sampling rate of 10 samples/sec, n_o is equal to one sampling unit and $\hat{m}(n)$ will have its cepstral peaks at every sample of $\hat{s}(n)$; hence even for the first few larger cepstral peaks of $\hat{m}(n)$, they cannot be distinguished from $\hat{s}(n)$. For a sampling rate of 40 samples/sec, n_o is equal to four sampling units, and $\hat{m}(n)$ will have its cepstral peaks only at every four samples of $\hat{s}(n)$; hence there might be better chance to differentiate among them.

3. Experimental Results

The cepstrum analysis was applied to two groups of synthetically-mixed signals with three different sampling rates: 10, 20, and 40 samples/sec. Since the NORSAR-recorded short period P-waves of presumed underground nuclear explosions from EKZ were available to us only at the sampling rate of 10 samples/sec, signals of 20 and 40 samples/sec must be obtained by some interpolation process. We implemented the interpolation process as a linear filtering process (Schafer and Rebiner, 1972) and applied it to the cepstrum-resolved P-phases which were obtained from a previous cepstrum analysis with a sampling rate of 10 samples/sec. Then, two groups of synthetically-mixed signals were constructed from these interpolated P-phases according to equation (I-16). In the first group, we made $t_o = n_o \Delta t$. Results of cepstrum analysis from this group will show the effect of different sampling rates on the detection of the P-pP delay time. In the second group, we made

$t_o = n_o \quad t \pm \frac{\Delta t}{M}$, with M = 2 and 4. This equation makes the delay time built into the sampled mixed signals to be a half or quarter sampling interval off the real delay time. Results of cepstrum analysis from this group will show the effect of missing the real delay time due to sampling on the detection of the P-pP delay time.

Figures I-2 through I-4 show the cepstra of the synthetically-mixed signals in the first group for sampling rates of 10, 20, and 40 samples/sec, respectively. The P-pP delay times built in these signals are t_o = 0.1, 0.2, 0.3, 0.4, 0.5, and 0.6 second, which correspond to n_o = 1, 2, 3, 4, 5, and 6 sampling units for a sampling rate of 10 samples/sec; which correspond to n_o = 2, 4, 6, 8, 10, and 12 sampling units for a sampling rate of 20 samples/sec; and which correspond to n_o = 4, 8, 12, 16, 20, and 24 sampling units for a sampling rate of 40 samples/sec. According to equation (I-17), the cepstral peaks due to the P-pP delay time -- i.e., m(n) -- should occur at $n = kn_o$ sampling units, k = 1, 2, 3,... . For a sampling rate of 10 samples/sec, it is noticed that the first cepstral peak at $n = n_o$ is mixed with the cepstra of the signal -- i.e., $\hat{s}(n)$ -- and cannot be identified for $t_o \leq 0.4$ second, although the second and the third cepstral peaks at $n = 2n_o$ and $3n_o$ stand out quite well from the surrounding cepstra for $t_o \geq 0.3$ second. For t_o = 0.5 and 0.6 second, there is no question of identifying the first three cepstral peaks. For a sampling rate of 20 samples/sec, the first cepstral peak starts to appear at t_o = 0.2 second and becomes clearer for larger t_o's. However, the later cepstral peaks, i.e., the second and the third, start to disappear at t_o = 0.5 second and are completely buried in the surrounding cepstra at t_o = 0.6 second. For a sampling rate of 40 samples/sec, the first cepstral peak is thought identifiable for t_o = 0.1 seconds, and it becomes better identified for larger t_o's. However, the later cepstral peaks are mixed with the surrounding cepstra and cannot be identified for $t_o \geq 0.4$ second.

The above observations indicate the following conclusions:

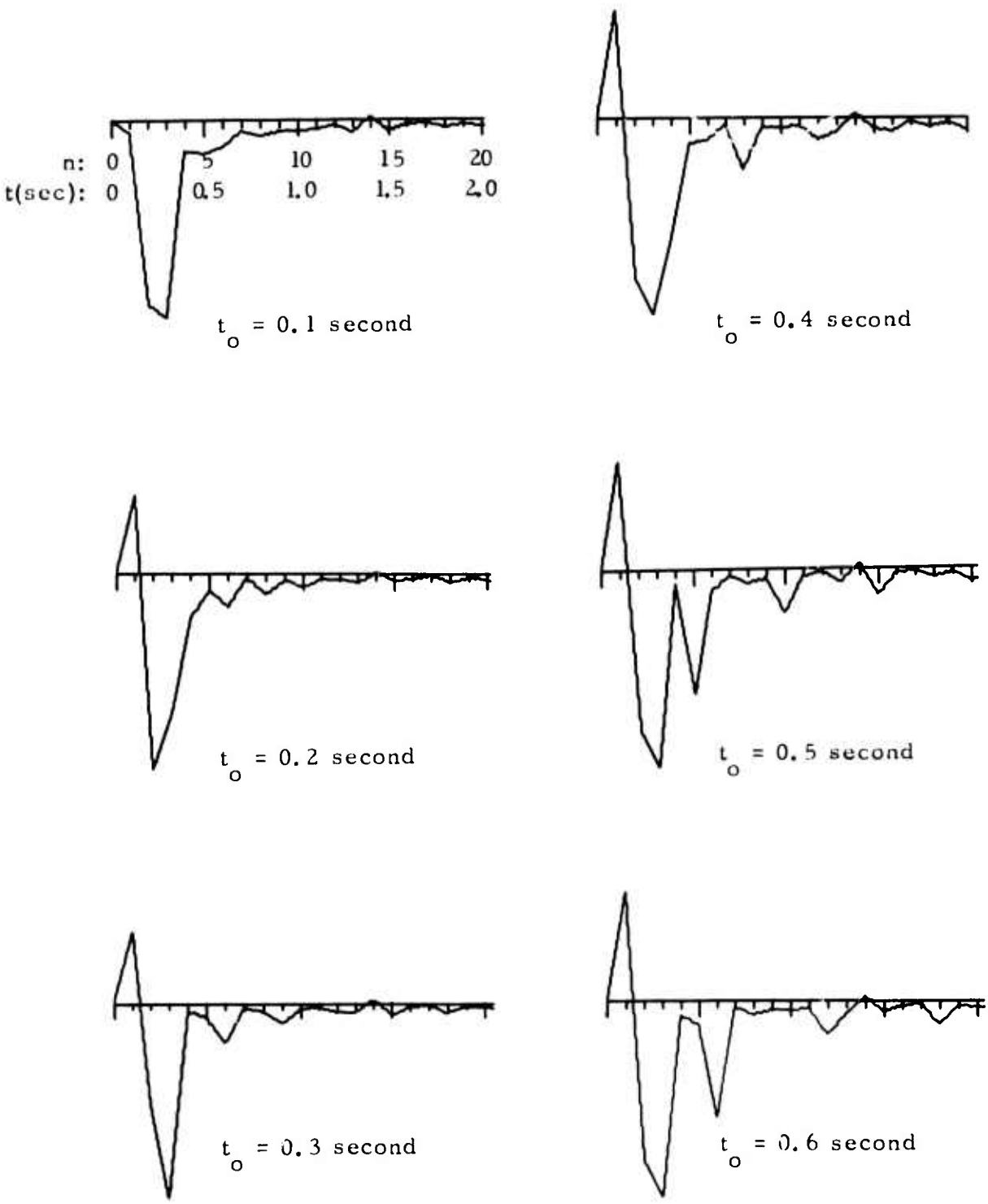

FIGURE I-2

CEPSTRA OF MIXED SIGNALS: $x(t) = s(t) - 0.9s(t-t_o)$
SAMPLED AT 10 SAMPLES/SEC

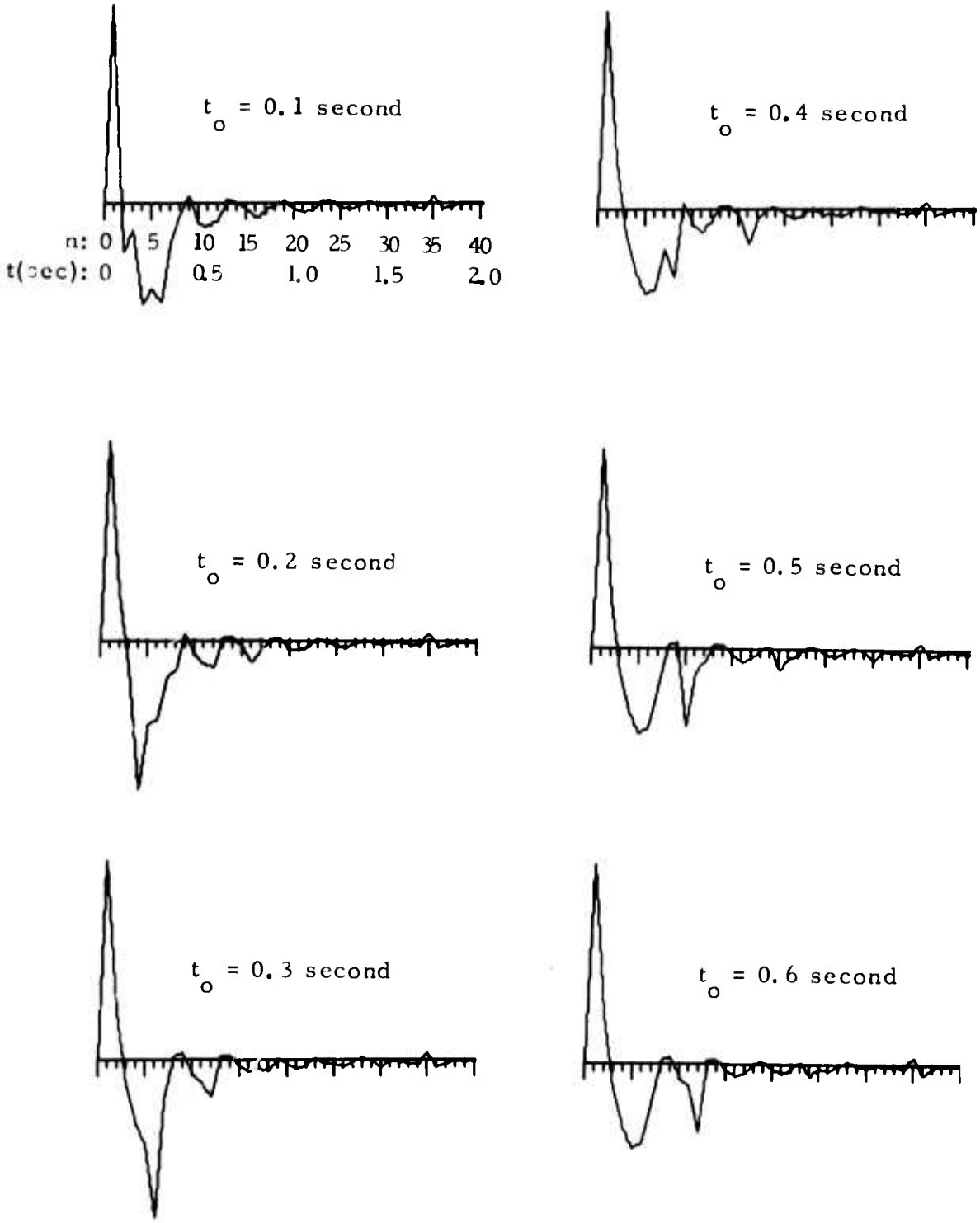

FIGURE I-3

CEPSTRA OF MIXED SIGNALS: $x(t) = s(t) - 0.9s(t-t_o)$
SAMPLED AT 20 SAMPLES/SEC

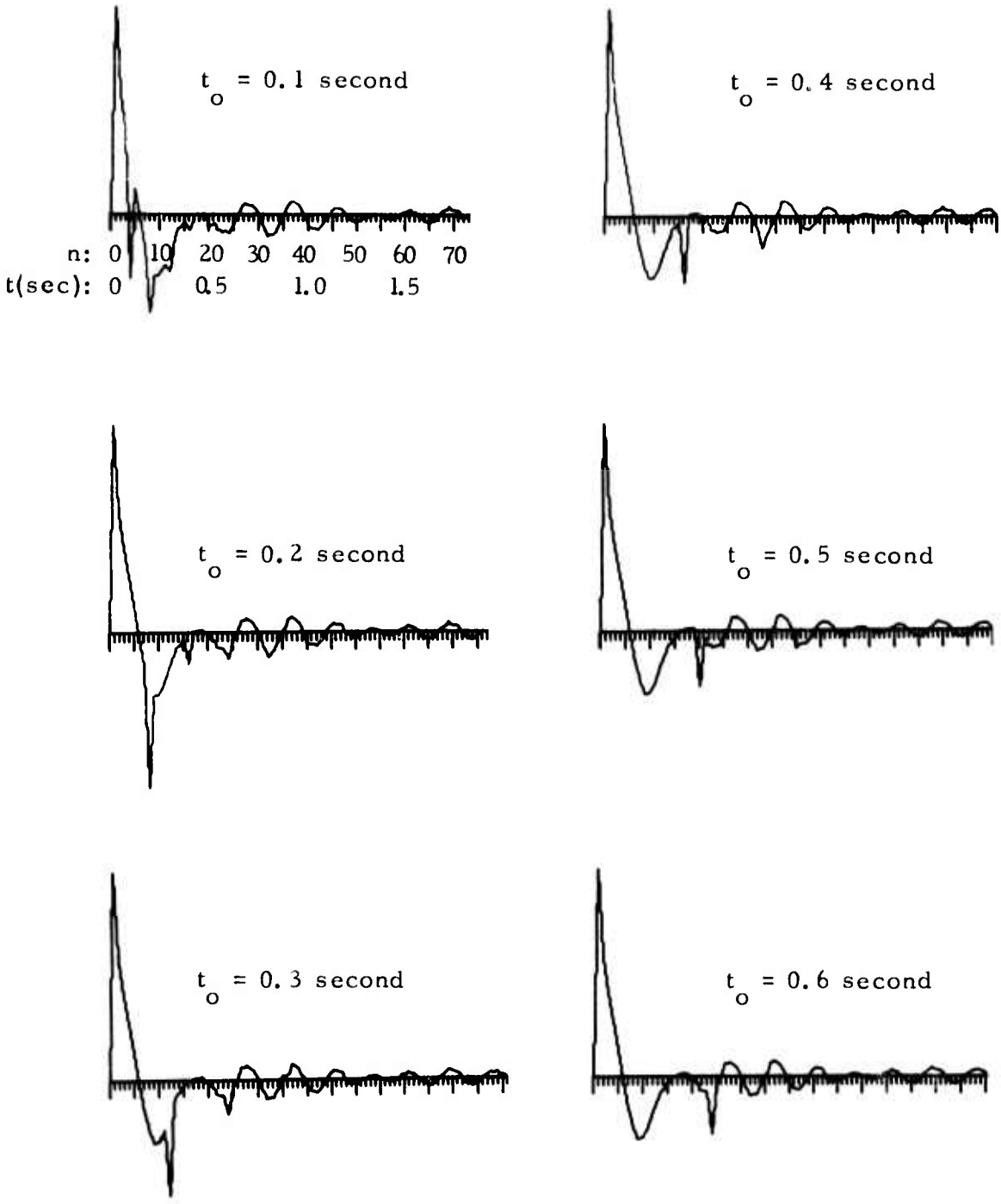

FIGURE I-4

CEPSTRA OF MIXED SIGNALS: $x(t) = s(t) - 0.9s(t-t_o)$
SAMPLED AT 40 SAMPLES/SEC

- For short P-pP delay time, $t_o \leq 0.4$ second, the identification of the first cepstral peak due to the P-pP delay time is better with a higher sampling rate.

- The shortest P-pP delay time which can be detected by identifying the first cepstral peak varies among different sampling rates. For the sampling rate of 10 samples/sec, it is 0.4 second (4 sampling units). While for the sampling rates of 20 and 40 samples/sec, they are 0.2 second (4 sampling units) and 0.1 second (4 sampling units), respectively. This suggests that the shortest P-pP delay time detectable by the cepstrum analysis does not depend on the P-pP delay time in the unit of real time, i.e., t_o seconds; rather, it depends on the P-pP delay time in the unit of sampling units, i.e., n_o sampling units. This shortest P-pP delay time for the class of signals that we analyzed here is 4 sampling units.

- For a longer P-pP delay time, $t_o > 0.4$ second, the identification of the cepstral peaks due to the P-pP delay time is better for lower sampling rate. It is believed that this is due to the extra high frequency noise introduced by oversampling.

The identification of the cepstral peaks due to the P-pP delay time constitutes just one part of the cepstrum analysis on a given short period P-wave. The other part is the decomposition of that signal into its P-phase and pP-phase by filtering in the cepstrum time domain. Thus, we applied a shortpass filter at $n = n_o$ to the cepstra shown in Figures I-2 and I-4. Results are presented in Figures I-5 through I-7. In each figure, the original mixed signal is given first and is followed by the cepstrum-resolved signals -- the first arrival (P-phase) in solid lines and the second arrival (pP-phase) in dashed lines. It is found that the shortest P-pP delay time in which the cepstrum analysis can successfully decompose the mixed signal into its P-phase

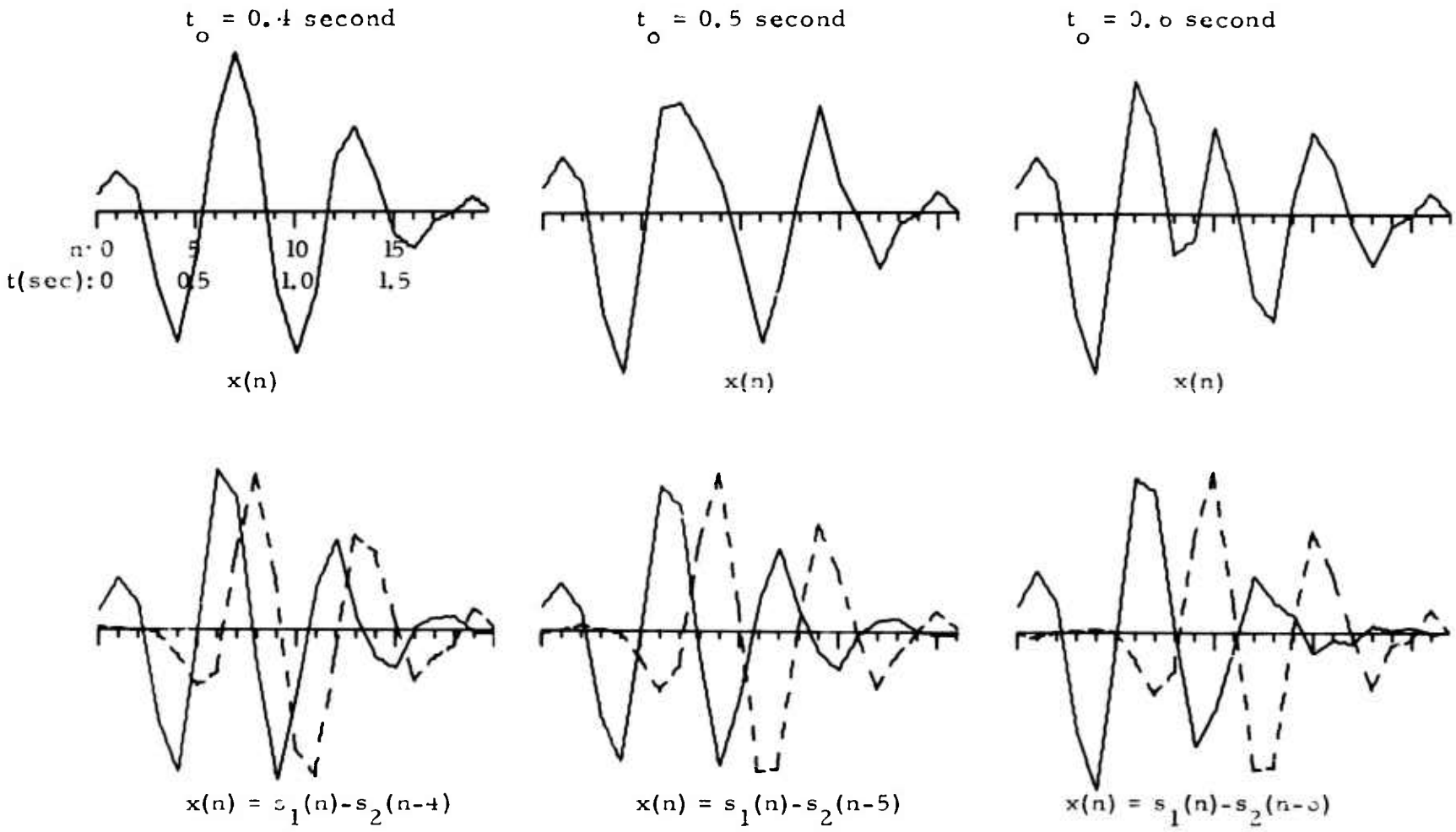

FIGURE I-5

CEPSTRUM DECOMPOSITION OF MIXED SIGNALS:
$x(t) = s(t) - 0.9s(t-t_o)$ SAMPLED AT 10 SAMPLES/SEC

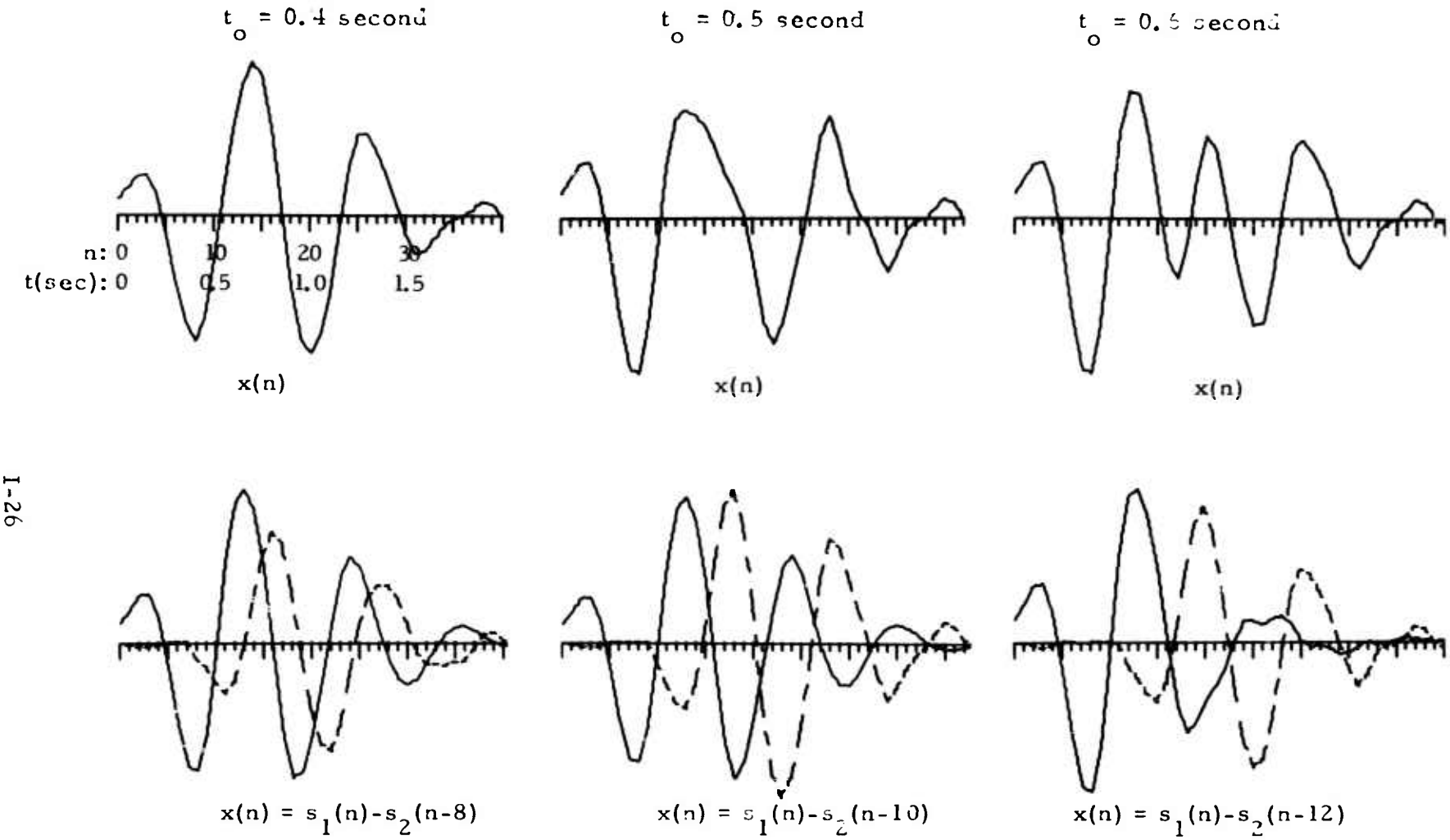

FIGURE I-6

CEPSTRUM DECOMPOSITION OF MIXED SIGNALS:
$x(t) = s(t) - 0.9s(t-t_o)$ SAMPLED AT 20 SAMPLES/SEC

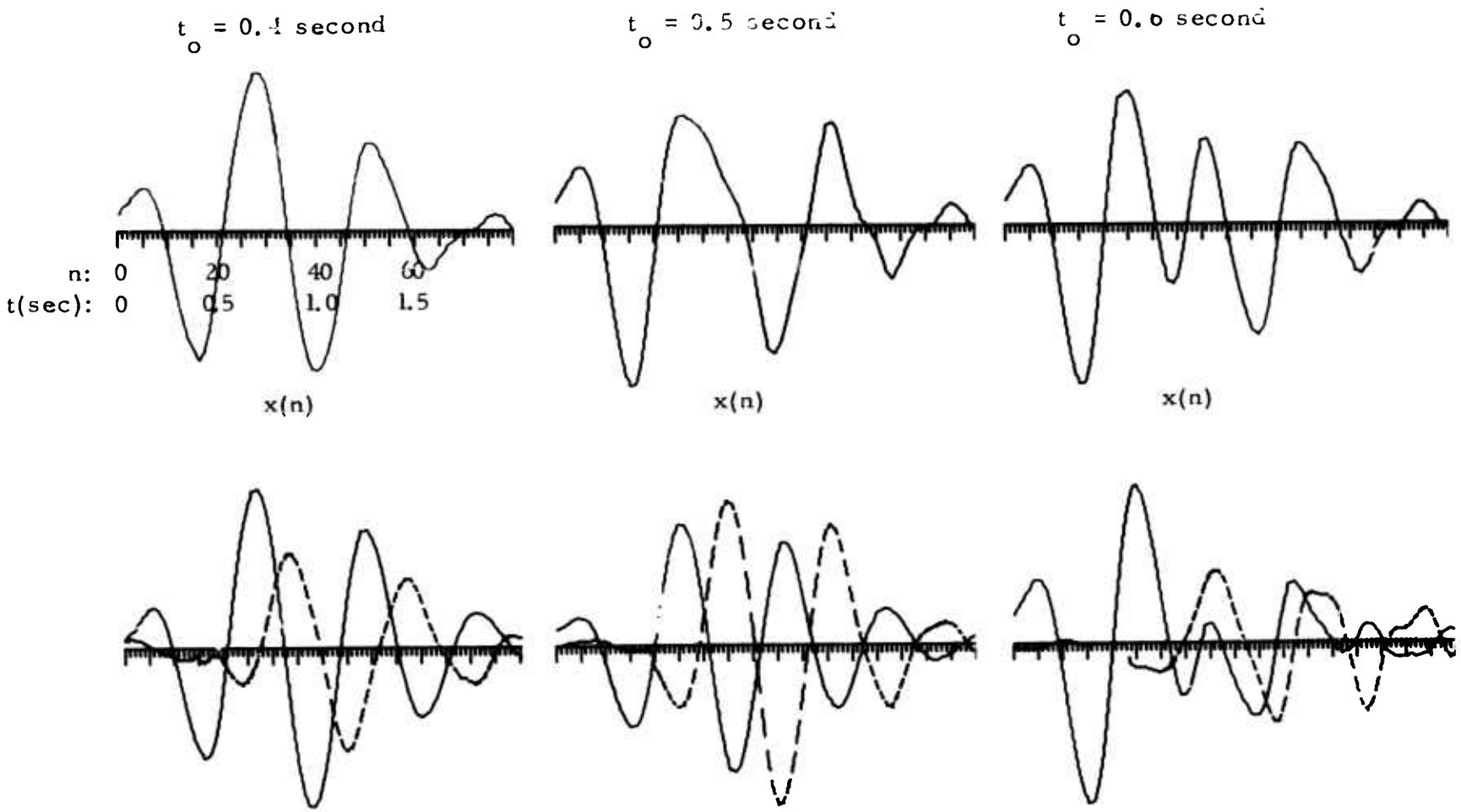

FIGURE I-7

UNSUCCESSFUL CEPSTRUM DECOMPOSITION OF MIXED SIGNALS:
$x(t) = s(t) - 0.9s(t-t_o)$ SAMPLED AT 40 SAMPLES/SEC

and pP-phase is independent of the sampling rate. This minimum P-pP delay time for the class of signals we analyzed here is 0.4 second. However, the quality of the resolved P-phase and pP-phase depends on the sampling rate. From examining Figures I-5 through I-7, it is fair to say that a sampling rate of 10 samples/sec yields the best quality. Again, it is believed that this is caused by the extra high frequency noise introduced by oversampling.

Figures I-8 through I-10 present the results of cepstrum analysis on the second group of synthetically-mixed signals for two cases of the P-pP delay time. In the first case, $t_o = 0.45$ and 0.55 second, and a sampling rate in 10 samples/sec. Thus, for this case, the exact delay time t_o is missed between two samples by a half sampling interval; i.e., $t_o = n_o \Delta t \pm 0.05$ second with $n_o = 5$ sampling units and $\Delta t = 0.1$ second (or, $t_o = n_o \Delta t + 0.05$ second with $n_o = 4$ sampling units, and $t_o = n_o \Delta t - 0.05$ second with $n_o = 6$ sampling units). The cepstra of the mixed signals are shown in Figure I-8. For comparison purposes, Figure I-10 shows the cepstrum of the mixed signal with a P-pP delay time t_o of 0.5 second and a sampling rate of 10 samples/sec. For $t_o = 0.5$ second, the cepstral peaks due to the P-pP delay time, i.e., $\hat{m}(n)$, occur exactly at $n = 5k$ sampling units, $k = 1, 2, 3, \ldots$, as expected. For $t_o = 0.45$ second, the first cepstral peak appears at $n = 5$ sampling units, while the second cepstral peak occurs at $n = 9$ sampling units. For $t_o = 0.55$ second, we notice only a broadened cepstral peak at $n = 5$ and 6 sampling units. Thus, it is clear that the missing of the exact P-pP delay time by a half sampling interval caused by sampling destroys the periodicity of the cepstral peaks due to the P-pP delay time, as indicated by $\hat{m}(n)$ in equation (I-17). Nevertheless, the first cepstral peak does occur at $n = n_o$ sampling units or $n_o \Delta t$ seconds, which is the best estimate of the exact P-pP delay time t_o.

In the second case, $t_o = 0.475$ and 0.525 second, and the sampling rate again is 10 samples/sec. Thus, the exact delay time t_o is missed between two samples by a quarter sampling interval, i.e.,

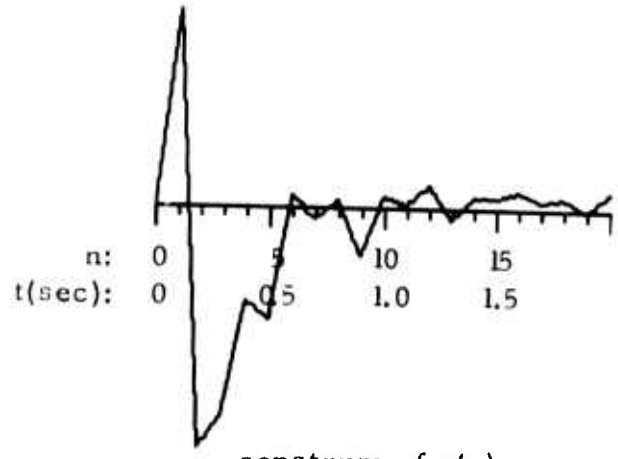

cepstrum of x(n)

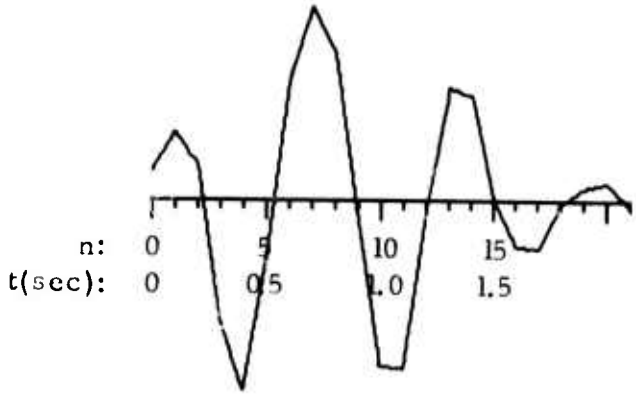

x(n)

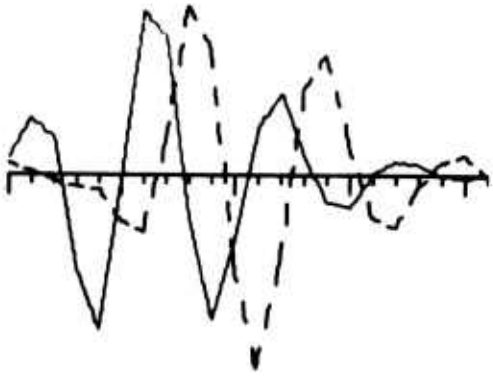

cepstrum decomposition: filtering at n=4 sampling units

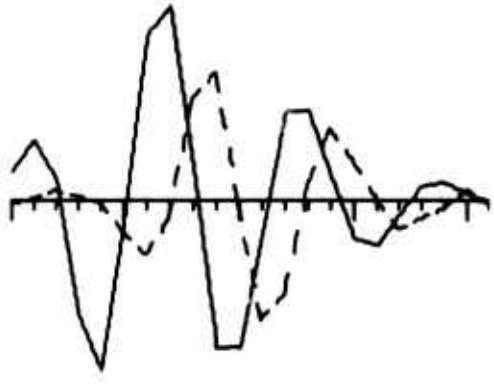

unsuccessful cepstrum decomposition: filtering at n=5 sampling units

FIGURE I-8a

CEPSTRUM ANALYZED RESULTS: $x(t) = s(t) - 0.9s(t-0.45)$
SAMPLED AT 10 SAMPLES/SEC
(PAGE 1 OF 2)

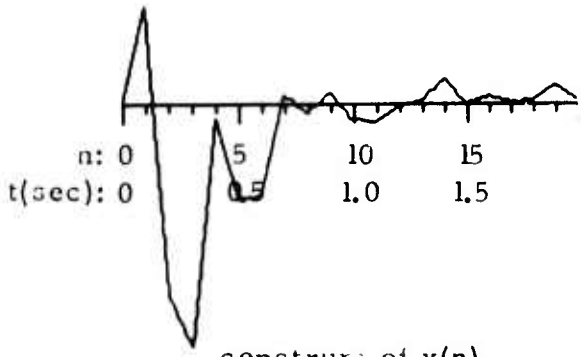

cepstrum of x(n)

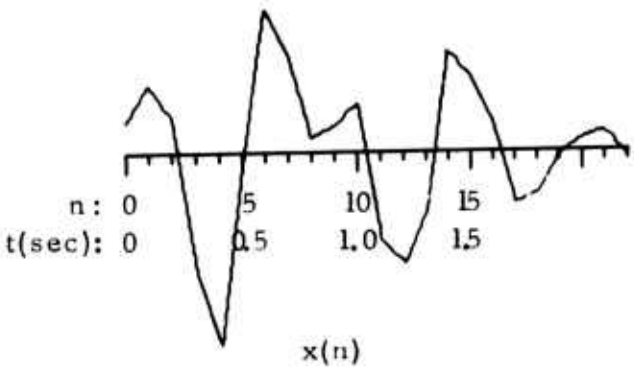

x(n)

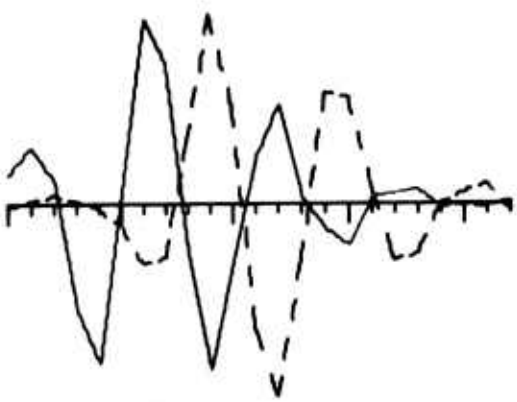

cepstrum decomposition: filtering at n=5 sampling units

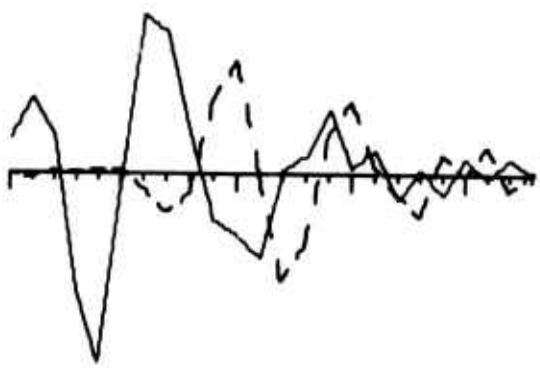

unsuccessful cepstrum decomposition: filtering at n=6 sampling units

FIGURE I-8b

CEPSTRUM ANALYZED RESULTS: $x(t) = s(t) - 0.9s(t-0.55)$
SAMPLED AT 10 SAMPLES/SEC
(PAGE 2 OF 2)

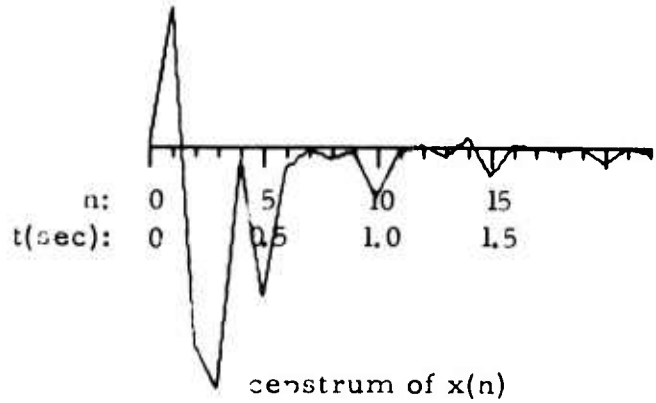

cepstrum of x(n)

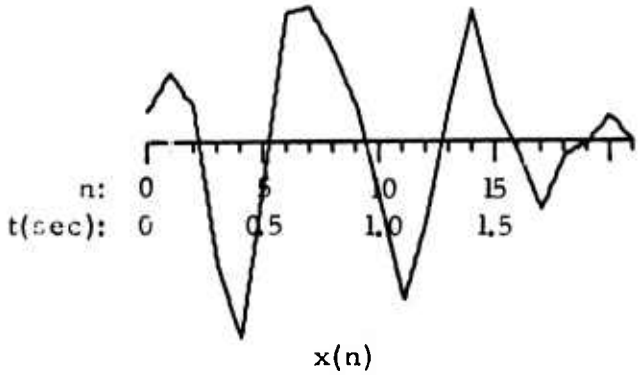

x(n)

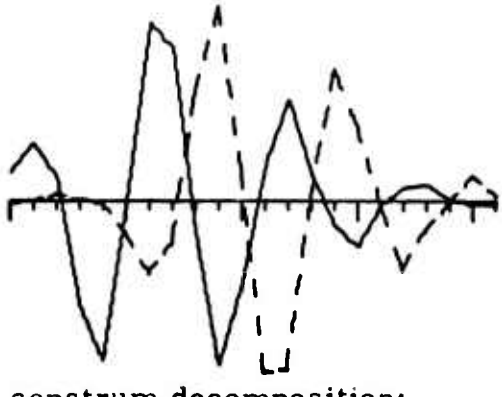

cepstrum decomposition:
$x(n) = s_1(n) - s_2(n-5)$

FIGURE I-9

CEPSTRUM ANALYZED RESULTS: $x(t) = s(t) - 0.9s(t-0.5)$
SAMPLED AT 10 SAMPLES/SEC

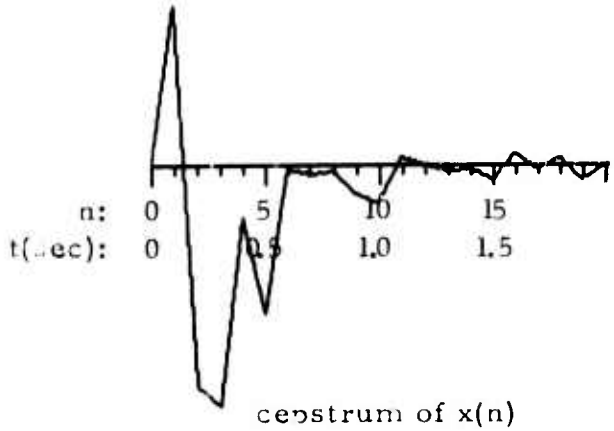

cepstrum of x(n)

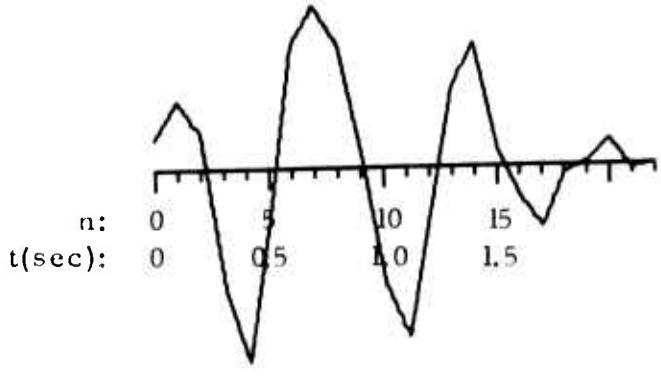

x(n)

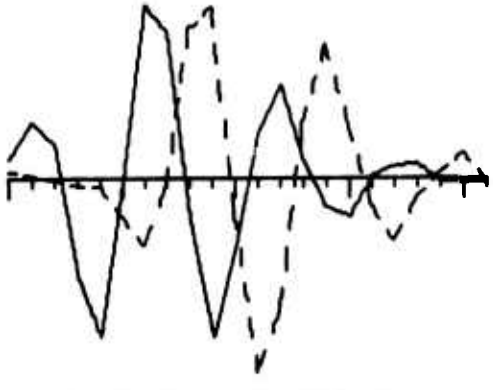

cepstrum decomposition: filtering at n=4 sampling units

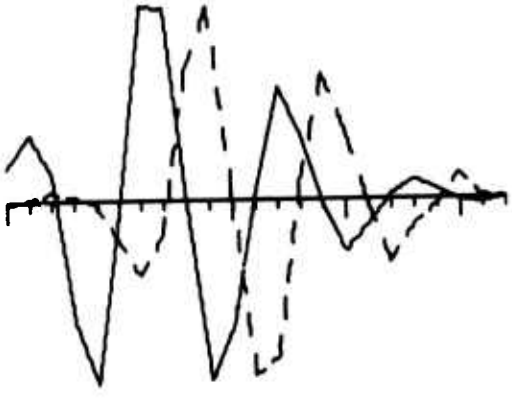

cepstrum decomposition: filtering at n=5 sampling units

FIGURE I-10a

CEPSTRUM ANALYZED RESULTS: $x(t) = s(t) - 0.9s(t-0.475)$
SAMPLED AT 10 SAMPLES/SEC
(PAGE 1 OF 2)

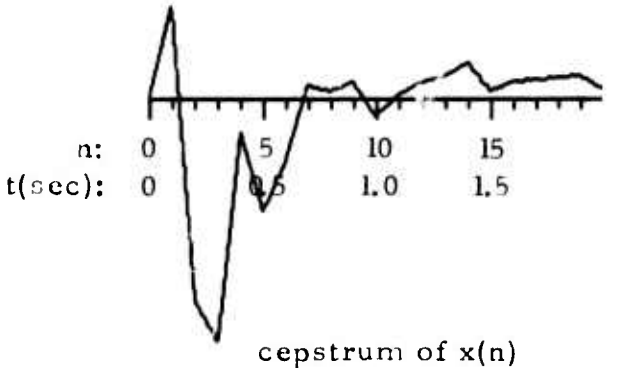

cepstrum of x(n)

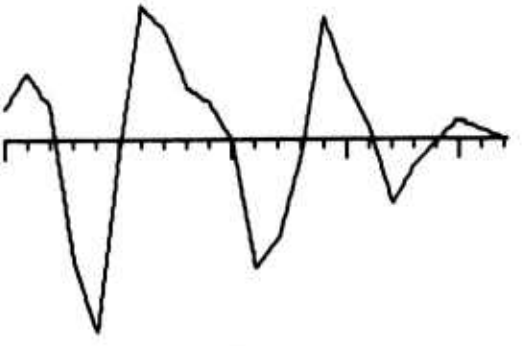

x(n)

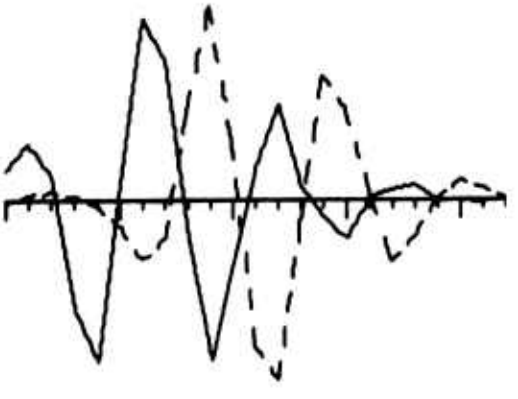

cepstrum decomposition: filtering at n=5 sampling units

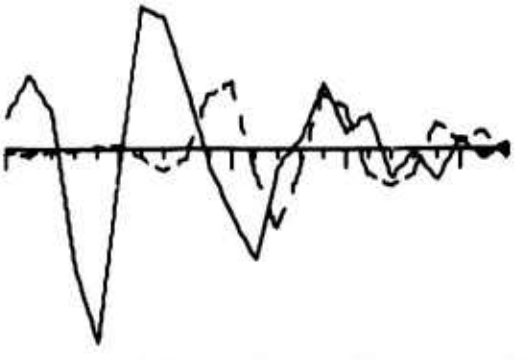

unsuccessful cepstrum decomposition: filtering at n=6 sampling units

FIGURE I-10b

CEPSTRUM ANALYZED RESULTS: $x(t) = s(t) - 0.9s(t-0.525)$
SAMPLED AT 10 SAMPLES/SEC
(PAGE 2 OF 2)

$t_o = n_o \Delta t \pm 0.025$ second with $n_o = 5$ sampling units and $\Delta t = 0.1$ second. The cepstra of the mixed signals are given in Figure I-10. It is noticed that the first two cepstral peaks occur at $n = 5$ and 10 sampling units. Comparing Figure I-10 with Figure I-9 where the exact P-pP delay time is retained in the sampling process, i.e., $t_o = n_o \Delta t$, it appears that the missing of the exact P-pP delay time by a quarter sampling interval due to sampling does not destroy the periodicity of the cepstral peaks due to the P-pP delay time. However, the period is not equal to the exact P-pP delay time t_o; rather it is equal to $n_o \Delta t$. Therefore, in both cases, especially in the first case, the detection of the P-pP delay time by identifying the corresponding cepstral peaks is not as clear as that for the case shown in Figure I-9. To confirm these detections, the shortpass filters are applied to these cepstra to obtain the possible decompositions of the mixed signals. The resulting cepstrum decompositions are shown in Figures I-8 through I-10. For the first case where the exact P-pP delay time is missed by a half sampling interval due to sampling, it is found that the successful cepstrum decomposition can be obtained only if the shortpass filter is applied at the cepstrum time, which is a half sampling interval earlier than the exact P-pP delay time; that is, the shortpass filter must be applied at $n = t_o/\Delta t - \frac{1}{2}$. However, for the second case where the exact P-pP delay time is missed by only a quarter sampling interval due to sampling, the successful cepstrum decomposition can be obtained by shortpass filtering at the cepstrum time when the first cepstral peak occurs.

4. Conclusions

The higher sampling rate is found to be helpful to detect the P-pP delay time by making the identification of the first cepstral peak due to the P-pP delay time more distinguishable from the surrounding cepstra, especially for the short P-pP delay time, $t_o \leq 0.4$ second. However, for the

longer P-pP delay time, $t_o > 0.4$ second, due to the high frequency noise introduced by oversampling, the higher sampling rate does not offer as clear an identification of the later cepstral peaks as the lower sampling rate.

Also, it is found that the shortest P-pP delay time detectable by the cepstrum analysis does not depend on the P-pP delay time in the unit of real time, i.e., t_o second; rather, it depends on the P-pP delay time in the unit of sampling units, i.e., n_o sampling units. This shortest P-pP delay time for the class of signals that we analyzed here is 4 sampling units. However, the shortest P-pP delay time that cepstral analysis can successfully decompose a mixed signal into its P-phase and pP-phase is independent of the sampling rate. This minimum P-pP delay time for the class of signals that we analyzed here is 0.4 second. Moreover, it is found that the missing of the exact P-pP delay time by a functional sampling interval due to the sampling process does not affect the detection of the P-pP delay time, as long as the detection is established both by identifying the cepstral peaks due to the P-pP delay time in the cepstrum time domain and by successfully decomposing the mixed signals into their P-phase and pP-phase in the time domain.

Finally, based on the study here, it is advised that the higher sampling rate be used, if it is available, for the identification of the cepstral peaks due to the P-pP delay time. For the cepstrum decomposition of the mixed signal, however, the lower sampling rate is more appropriate.

SECTION II
FAR-FIELD STUDIES

A. INTRODUCTION

In these studies, an effective methodology for determining seismic source parameters from teleseismic surface wave amplitude spectra was developed. Using a double-couple source buried in a plane layered half-space, exhaustive, iterative regression, and amplitude ratio spectral fitting procedures were applied to many earthquakes with varying degrees of success. For earthquakes originating in continental structures with shallow focal depths (<10 km), adequately recorded and corrected for path effects, it is felt that the source depth can be determined to within a few kilometers.

In Subsection B, the main conclusions of the source parameter study are presented. The conclusions from the attenuation studies using teleseismic surface wave and body wave data are given in Subsection C.

B. SEISMIC SOURCE PARAMETERS FROM TELESEISMIC SURFACE WAVE AMPLITUDE SPECTRA

The conclusions from this study can essentially be divided into three categories. The first is concerned with the examination of theoretical sources in a layered half space, and the examination of spectra from these sources for characteristics indicative of source depth and orientation. The second category describes the techniques used to obtain source parameter estimates by obtaining a least-squares fit of a double couple source in a plane-layered half space to observed surface wave spectra. The final

category reviews the application of these fitting techniques to events which have varying degrees of corroborative evidence to substantiate their source parameter estimates.

1. Examination of Theoretical Source Characteristics

Using the formalism of Ben-Menahem and Harkrider (1964), the general form for far-field Rayleigh and Love waves from a multipolar source in a layered half space may be written as follows:

$$\bar{U} = |R||n| k_\eta^m \, e^{-i(1 + 2m)\pi/4} \, N(h) \, X(\theta, h) \, e^{ikr} \qquad \text{(II-1)}$$

where:

k_η^m	is either k_R or k_L (m is the source order number),
$N(h)$	is either $N_\theta(h)$ or $N_{RZ}(h)$ (layer transfer function),
$X(\theta, h)$	is the complex valued function of the radiation pattern,
$\|R\|$	is the displacement in the plane of motion, and
$\|n\|$	is the unit displacement normal to plane of motion.

From the examination of fundamental and first higher mode Rayleigh and Love wave double-couple and quadrapole spectral plots generated using equation (II-1) (Turnbull et al., 1974b, 1975a, 1975b; Turnbull, 1976), the following conclusions were reached:

- The general form of the higher order source term remains essentially the same as that of the double couple. The major differences occur with the wavenumber k_η^m term, whose power increases as the order of the term, and the radiation pattern $X(\theta)$ term which becomes a more complicated function. A preliminary estimate of the relative importance of the higher order terms can be found in examining (1) the values of the wavenumber k_η for fundamental and higher mode surface waves, and (2) the geometry of the source. The

wavenumber term k_η^m in the quadrapole and higher order terms does not make a significant contribution until short periods (< 5 sec) for first higher mode waves. Also, the importance of these higher order multipoles, when considered as part of a volume source representation, will have coefficients which are possibly frequency dependent (for a non-separable source function) and representative of the source geometry. These higher order effects will probably manifest themselves in radiation pattern asymmetry.

- An alternative representation of a fault of significant extent with a finite rupture velocity can be obtained using multiple double couples with different origin times. Using a solution to the San Fernando earthquake of 1971, four double couples placed in a representative source structure produced highly asymmetric fundamental mode radiation patterns. An example of this asymmetry is shown in Figure II-1.

- Considering the spectral variation of both the double couple and quadrapole with respect to the source parameters, source depth variations produced the largest changes in spectral shapes and spectral levels. This was found to be true for the fundamental and first higher modes. The next largest variation is found with strike changes, with changes of dip and slip giving the smallest change of spectral level. For both source types, the spectral level of the fundamental mode over its period range of maximum excitation (10 to 50 seconds) is generally an order of magnitude greater than the first higher mode over its period range of maximum excitation (3 to 15 seconds). For both mode types, the spectral levels between the double couple and the quadrapole are usually an order of magnitude,

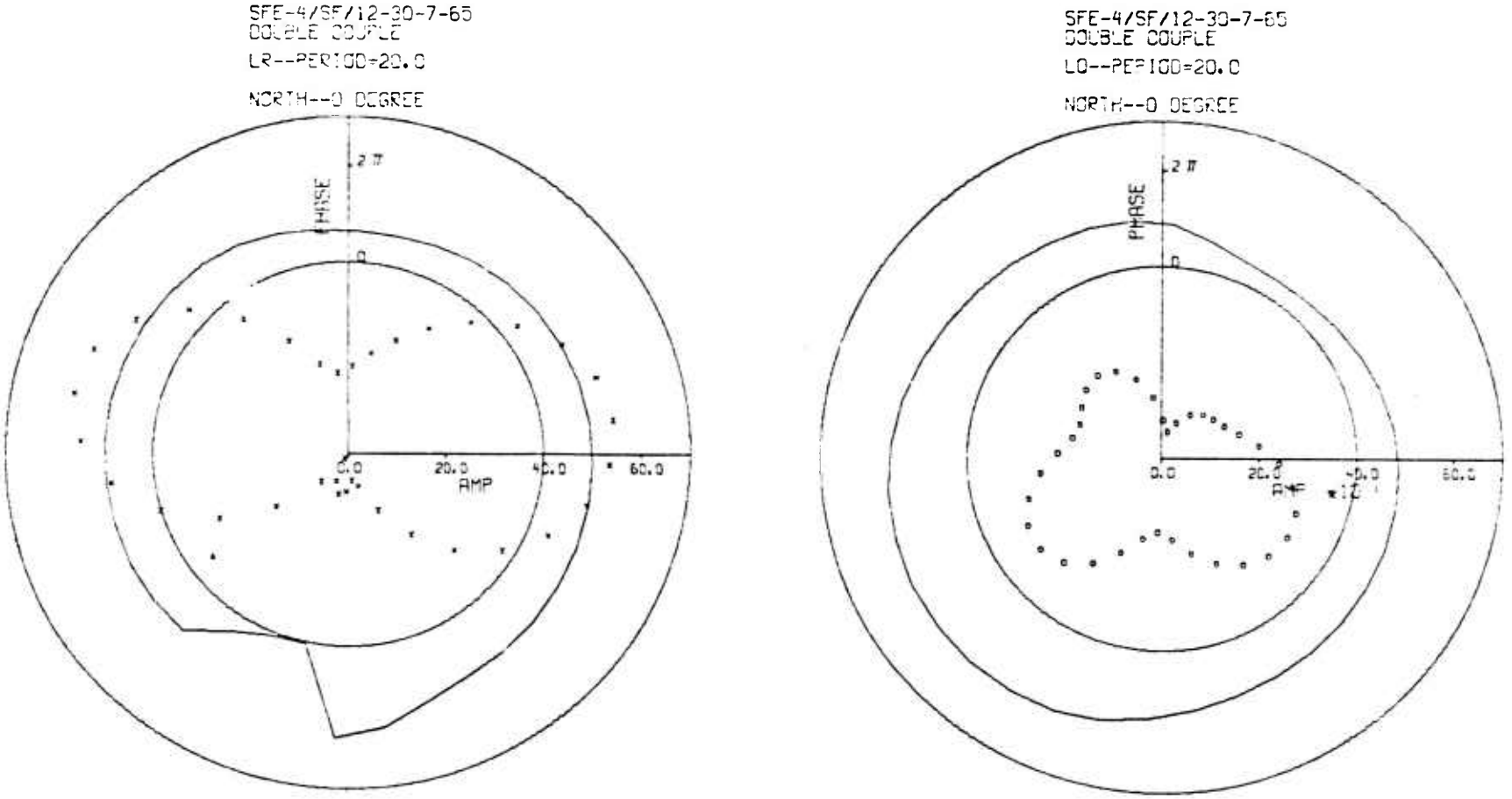

FIGURE II-1

FUNDAMENTAL MODE RAYLEIGH AND LOVE WAVE
RADIATION (T = 20 sec) USING A MULTIPLE DOUBLE COUPLE SOURCE
MECHANISM FOR THE 9 FEBRUARY 1971 SAN FERNANDO EARTHQUAKE

the double couple being the larger. Since special features of the spectral shape are important in the fitting of the observed spectra, a methodical investigation was carried out for their identification. An example of the three-dimensional spectral plots used for this investigation is shown in Figure II-2. For both source types, the largest changes in spectral level occur in the 10 to 20 seconds period range for the fundamental mode and 9 to 12 seconds for the first higher mode. Spectral holes occur for several particular fault parameter combinations, the most prominent for both source types and Rayleigh modes only when the fault is vertical strike-slip. These holes also occur, but are smaller in magnitude, when the slip angle is 90^{o} or the negative of the dip angle. For the most part, the holes occur when the source parameters produce a cancelling of some of the terms in the expression for the double-couple Rayleigh wave radiation.

- Various combinations of double-couple surface wave spectra for the fundamental and first higher modes were examined for characteristics of invariance with respect to source parameter variations in order to develop procedures for obtaining improved surface wave magnitudes. It was found that for all except very shallow sources (~5 km), the most reliable estimates of surface wave magnitude can be obtained from azimuthal averages of total surface wave energy, $R^2 + L^2$, of the fundamental mode. An example of this invariance is shown in Figure II-3, where the total fundamental mode surface wave energy is plotted as a function of source depth, dip angle, and slip angle. The invariance is obvious from the large spectral overlap. The first higher mode offers very little opportunity for an improved surface wave magnitude estimate. For shallow

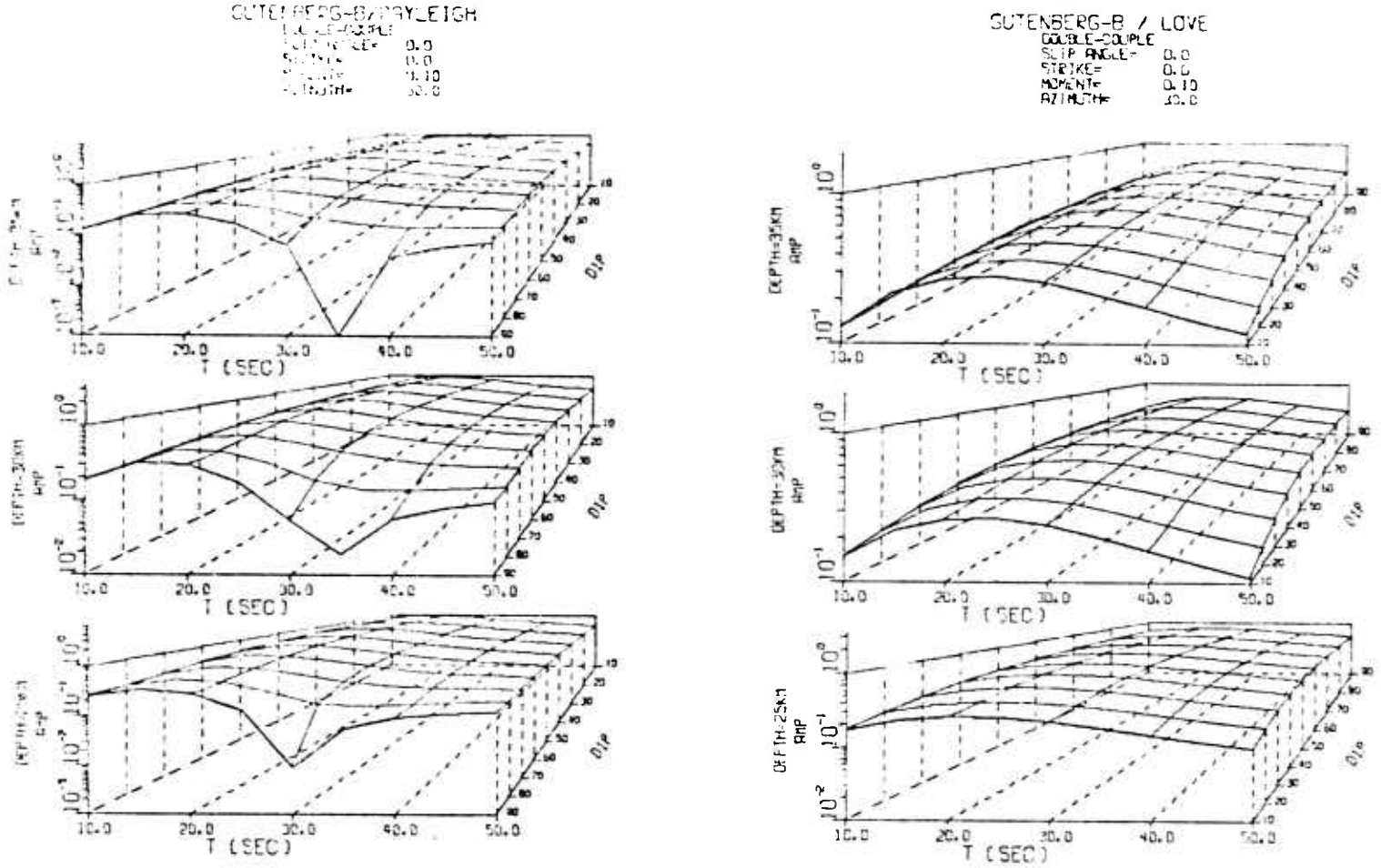

FIGURE II-2

FUNDAMENTAL MODE DOUBLE COUPLE RAYLEIGH AND LOVE WAVE AMPLITUDE SPECTRA FOR A GUTENBERG-BULLEN EARTH MODEL (h = 25, 30, 35 km, δ = Variable, $\lambda = 0^{\circ}$, $\theta = 0^{\circ}$, $\phi = 30^{\circ}$)

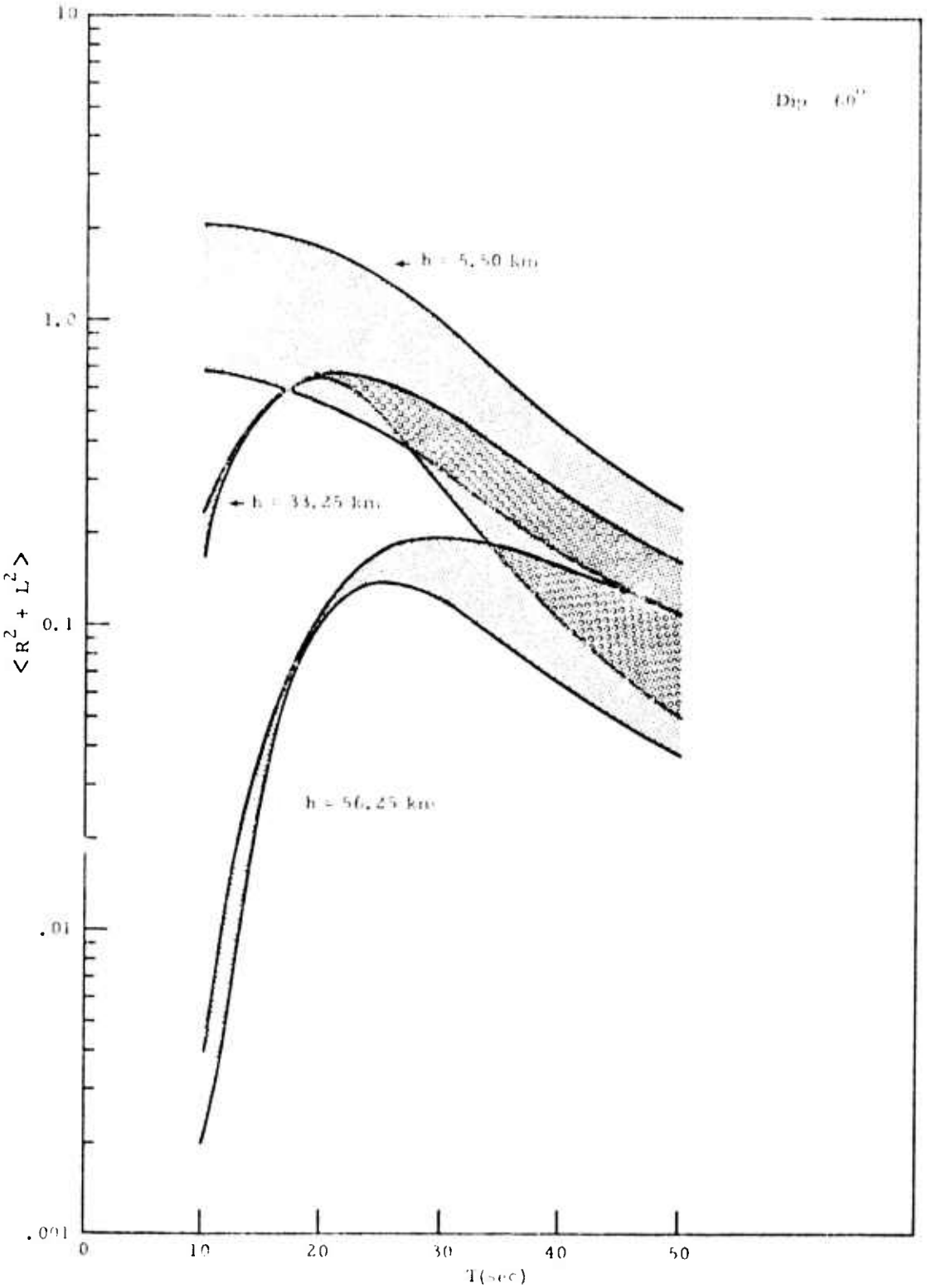

FIGURE II-3

AVERAGED FUNDAMENTAL MODE RAYLEIGH SQUARED PLUS LOVE SQUARED (R^2+L^2) AMPLITUDE SPECTRA FOR 3 DEPTHS, THE FULL RANGE OF SLIP ANGLES (SHADED AREA), AND DIP ANGLE OF 60°

sources it is best to use an azimuthal average of fundamental mode Rayleigh waves alone, R^2, preferably in the period range 20 - 30 seconds. Finally, the effects of radiation patterns on magnitude can be satisfactorily minimized by averaging about 8 stations distributed over any 180^o sector of azimuth.

2. Development of Techniques to Fit Far-Field Surface Wave Amplitude Spectra for Determination of Source Parameters

Three methods for fitting far-field surface wave amplitude spectra were developed in these studies. The first was a refined version of Tsai and Aki's (1970) exhaustive comparison technique between the observed and theoretical spectra. Modifications to this technique included a rearrangement of the order in which the parameters are varied, and the generation of a detailed knowledge of the minimum residual distribution. This latter modification is helpful in determining the distribution of solutions about the absolute minimum and guards against a possible spurious minimum generated by poor quality data.

The second method developed was an iterative regression procedure (Turnbull et al., 1973; Turnbull, 1976). The source parameters which easily lend themselves to this type of regression analysis are the dip angle (δ), slip angle (λ), strike angle (θ), and seismic moment (M). Including source depth (h) in this procedure was found to be impractical, because of the complicated variation of the layer response functions (N_{ij}). The depth was usually approximated using independent information such as pP. Using initial choices of the source parameters guided by independent source information (such as bodywave fault plane solutions), regression proceeds as to precise a solution as is desired at several depths close to the approximate value. The parameters which produce the absolute minimum residual become the source solution.

The third method involves integrating either of the two previously described procedures into the 'master' event concept. The master event can be thought of as any event which has well recorded data and a documented source mechanism solution. Then if another event occurs in the same region, possibly of lower magnitude, and is recorded on the same set of stations, amplitude spectral ratios can be used in the fitting procedures. The dividend obtained from this approach is the virtual elimination of source-station travel path effects and instrument response effects.

Applying the first two spectral fitting procedures to test cases, the following conclusions were reached:

- The improved exhaustive fitting procedure was tested by attempting to fit a theoretical explosive source using Rayleigh waves only. Implementing several azimuthal combinations, one particular double-couple source configuration was obtained in every case. Comparing this spectra to that of the explosive source, a very close match was obtained in both spectral level and shape, even though the double-couple source was 15 km deep. Of course, the associated Love wave radiation pattern for the double couple was highly non-circular and thus indicated the source was an earthquake. A factor which detracts from implementing this procedure was manifested in this test case, that a rather lengthy computer run time (45 minutes on an IBM 360/44).

- From testing the iterative regression scheme on theoretical double-couple spectra using a restricted source depth, the initial values of the source parameters can be as much as 30^{o} off the actual values (and a factor of 3 to 5 off for the seismic moment). Typical computer run time is under 6 minutes. The minimum azimuthal spread needed for convergence was found

to be 90°. Perturbing the theoretical spectra using a random number generator to simulate incorrect path and instrument corrections did not appreciably affect the final result.

3. Application of the Spectral Fitting Techniques

Both the iterative regression and exhaustive spectral fitting schemes were applied to well recorded and documented events after the data had been corrected for instrument and path effects. Then the exhaustive scheme was applied to events with fewer recordings and less documentation. Finally, the 'master' event concept, using amplitude spectral ratios, was applied to pairs of events with common source-station paths. From this analysis the following major conclusions were reached:

- Analysis of the Southeastern Missouri Earthquake of 21 October 1965 using both methods yielded solutions very close to the existing surface wave and bodywave solutions (Turnbull et al., 1973). Several representative earth models with highly different crustal structures were used, with a resultant variation of only 2 km in the focal depth estimate.

- The minor variation of focal depth with crustal structure was quite puzzling until theoretical spectra were generated using several different crustal models (Turnbull, 1976). It was found that fundamental mode shape and spectral level for very shallow sources varies little with crustal structure. For depths greater than 10 km, the structural responses are quite different in terms of spectral level. The existence of spectral holes and other special characteristics do not vary significantly in the fundamental mode spectra for different continental earth models. For the higher mode spectra, though, both the level and shape varied significantly with the earth model.

- Analysis of well recorded events having independent source information was quite successful, with parameter estimates reasonably close to the independent values. For an Eurasian event, the analysis of a travel path along the Alpine-Himalayan fold system yielded large group velocity delays (~0.5 km/sec less) and almost twice the normal energy attenuation coefficient. Analysis of the Bear Valley event of 22 June 1973 using only 3 stations resulted in a source mechanism surprisingly close to the very near-field source solution (Turnbull et al., 1975a). The one significant difference is in the moment estimate, which is an order of magnitude smaller than the near-field estimate. Both the near- and far-field solutions agree with the respective solutions of other investigators for this event.

- Pairs of events were analyzed using both spectral fitting of the individual event spectra and fitting using spectral ratios. These pairs have minimal independent source parameter estimates, but do have very close epicenters and common stations within each pair. The agreement between the individual and spectral ratio solutions was quite close, especially in terms of source depth. One of the pairs, located in Eurasia, had the identical Alpine-Himalayan path mentioned above (Turnbull, 1976). Because the individual and spectral ratio solutions agreed, the effective attenuation estimate for this path was confirmed.

C. ATTENUATION STUDIES

The results of two somewhat different investigations are presented here under the broad title of "Attenuation Studies." The first topic is concerned with the determination of effective attenuation for selected travel paths using surface wave data. The second topic is a comparative analysis of upper mantle Q and other geophysical data on the Eurasian continent. The common thrust of both studies is the understanding of the effects of travel paths and of earth structures on seismic measurements used for discrimination purposes.

1. Determination of Effective Attenuation Using Far-Field Surface Wave Data

Rayleigh wave energy attenuation coefficients in the period range of 10 to 50 seconds were estimated for many travel paths by applying the two-station method and Tryggvason type methods to earthquake and explosion data. In general, the results are thought to be realistic. However, no attempt was made to interpret the obtained attenuation curves in terms of earth structure Q values. The computed attenuation coefficients were used for traval path attenuation corrections in the estimation of far-field source parameters and possibly in the calculation of surface wave magnitude. Based on the knowledge gained from this attenuation study, the following conclusions may be stated:

- Although the two-station method is mathematically simple, its practical application is limited because it is hard to find two stations which lie exactly on the same event-station great circle path. Serious error in the computed energy attenuation coefficient can be made when the source azimuths of two stations are not exactly the same or are close to the nodal direction of the surface wave radiation pattern.
- Noticeable differences in the frequency variation of the computed attenuation curve can be expected between different

travel paths. Hence, it seems that the attenuation coefficients obtained for a specific travel path by the two-station method can, at best, be used only along that path.

- Because of the scarcity of reliable data which could be used by the two-station method, the Tryggvason (1965) approach was used to obtain average effective attenuation values for travel paths of interest. The basic assumptions used by this approach are that the radiation pattern from the source is approximately circular and that the event is recorded by many stations. Using the observed spectra at these stations, both a least-squares fit for each frequency of interest and effective energy attenuation coefficients were obtained. Of course, this approach works best for explosions, but can be applied to earthquake data with reasonable success. An interesting example of the application of this method is shown in Figure II-4, where the effective attenuation for a travel path from Eastern Kazakh to Chiang Mai, Thailand, has been estimated (Turnbull et al., 1973, 1974a). Because of either scattering or absorption effects when the surface waves pass through the Himalayan Fold System, the effective attenuation was found to be at least twice as large as that normally observed for continental travel paths.

- A modified Tryggvason approach was developed by Sun (1976) using a small number of stations with many events from the same source region. This approach yielded results comparable to those obtained by using a large number of observation stations with a single event. However, when using this modified approach, the data quality should be good and consistent among the events; otherwise, the computed k_e values can be physically unrealistic.

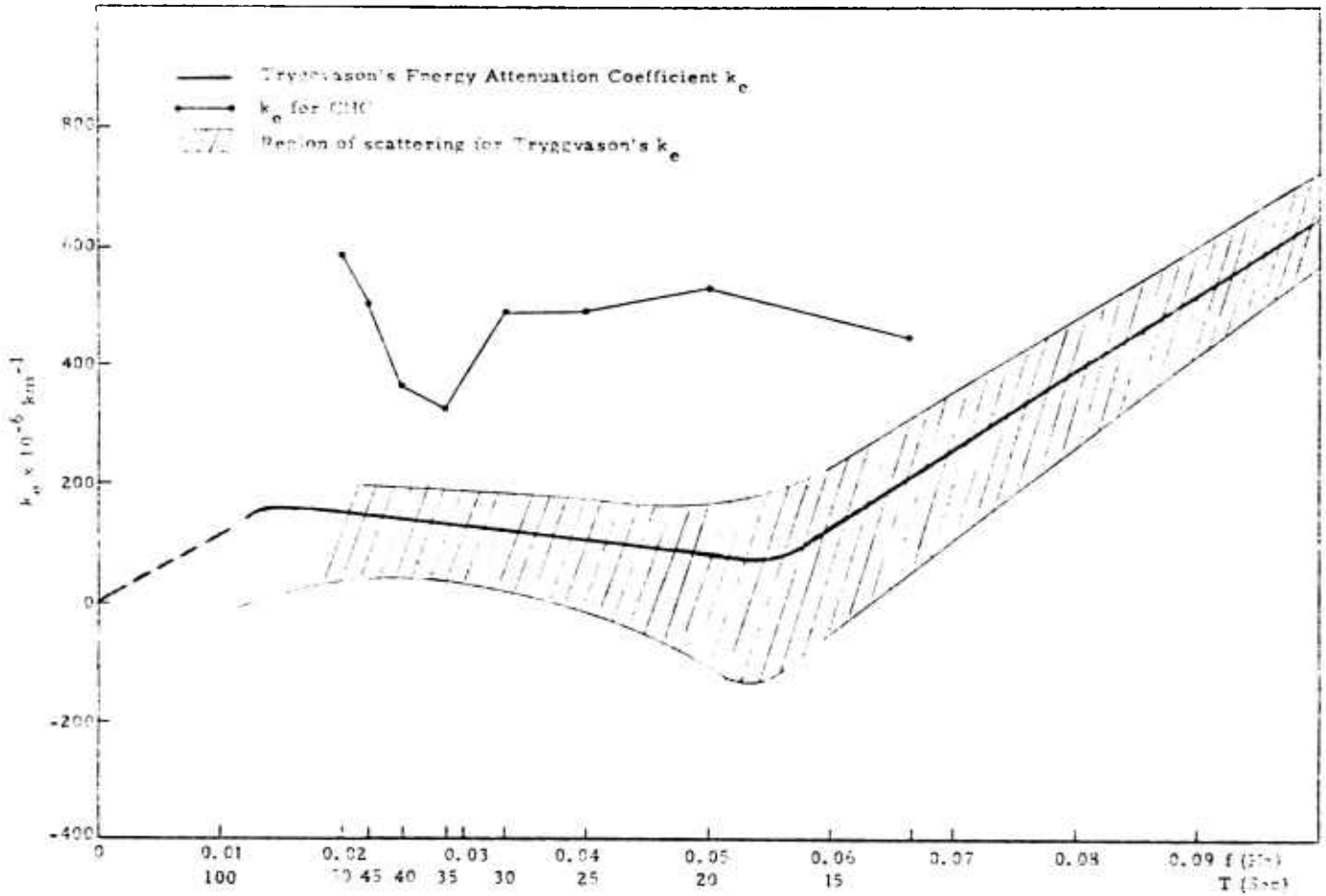

FIGURE II-4

TRYGGVASON'S ENERGY ATTENUATION COEFFICIENT FOR EURASIA IN GENERAL AND FOR PATH ALONG ALPINE-HIMALAYAN FOLD TO CHG

- The average Rayleigh wave attenuation coefficients estimated from the NTS events for travel paths from NTS to the array stations (ALPA, NORSAR, LASA) agree quite well with Tryggvason's attenuation curve, although the former has a slightly higher value for short periods.

- Based on observed Rayleigh wave data used in these studies, large energy attenuation coefficients were obtained for travel paths from the eastern Kazakh to the three array stations. Although this approach seemed unusual, the data was reliable enough to make this conclusion.

2. Comparative Analysis of Upper Mantle Q and Other Geophysical Data on the Eurasian Continent

Characteristics of seismic bodywave propagation within Eurasia are influenced by geophysical parameters along the propagation path which are not directly observable by stations collecting recordings outside or around the borders of the Eurasian land mass. There are, however, translations of scientific reports or reports prepared in English which concern measurements and interpretations of geophysical data collected in Eurasia which may offer some insight into factors which are known to represent or to have influence on seismic bodywave propagation conditions. This study (Alsup, 1973) included the results of a literature survey for collecting pertinent Eurasian geophysical data into a brief reference document which can serve as one guideline for interpretation of anomalous signal features or identify regions or paths which may cause anomalous signal features or identify regions or paths which may cause anomalous signal behavior.

Data from Eurasian sources appear to coincide with observations in the U.S. and other regions in terms of the qualitative corroborations found among geotectonics, P-wave velocities in the upper mantle, heat flow from within the earth, telluric current influences, and P-wave absorption.

The broad continental structural platform comprising most of the USSR is apparently supported by a relatively stable and rigid upper mantle where high P-wave velocities and low absorption for P-wave energy is representative. Around the peripheries of this broad region are localized zones of slow velocities and strongly absorptive characteristics. No broad region of high attenuation similar to the Basin and Range Province of the U.S. is evident, unless the Sea of Okhotsk - Sea of Japan-Kurile-Kamchatka region is a representation of that province for Eurasia.

With the exception of areas around Lake Baykal and some of the small platform basins of south central USSR, the high P-velocity-low-absorption regions extend from the northern limits of the land mass to the front of the mountain ranges in southern Russia, and to the southern parts of the Caspian and Black Seas. Based upon the patterns of P-delays, northeastern China is similar in character, but P-wave absorption and heat flow probably increase toward western and southern China while upper mantle P-velocity should decrease. The complexities of the Himalayan regions were not resolved by the data on hand to any great extent. Heat flow in India is enigmatic, since the shield area should be considerably cooler and show less positive P-delays on the basis of observations on all other shield areas. The unique interpretation of the role of India in global tectonics as a battering ram on southern Eurasia may be related to this situation.

Details of heat flow and P-wave absorption in the eastern or border regions of Eurasia generally conform to observations of similar tectonic regions along the Pacific borders, with high heat flow and strong energy absorption beneath the Penninsula and island chain. The overall tectonic activity of the region would imply that local variations should exist, and variability in both factors within the regions seems to agree with such an implication. Relatively few teleseismic P-delays are available for interpretation here, but these are also somewhat variable. Numerical values of

absorption calculated here agree with those published by the Russian research groups, and there seems to be no reason to suspect that the tectonic effects of the island arc are different here than for similar regions elsewhere.

A regional map of estimated upper mantle Q for P-waves beneath Eurasia is given in Figure II-5 based upon the available data. The map cannot be considered a definitive display of values of Q, but should be used as a regional estimate which represents the best estimate derived from rather scanty data and subjective extrapolation over a very large geographic area. General characteristics of the relative upper mantle Q distribution beneath Eurasia are represented, however, and the map can serve as a guideline for further detailed analysis and corroboration for surface wave Q studies.

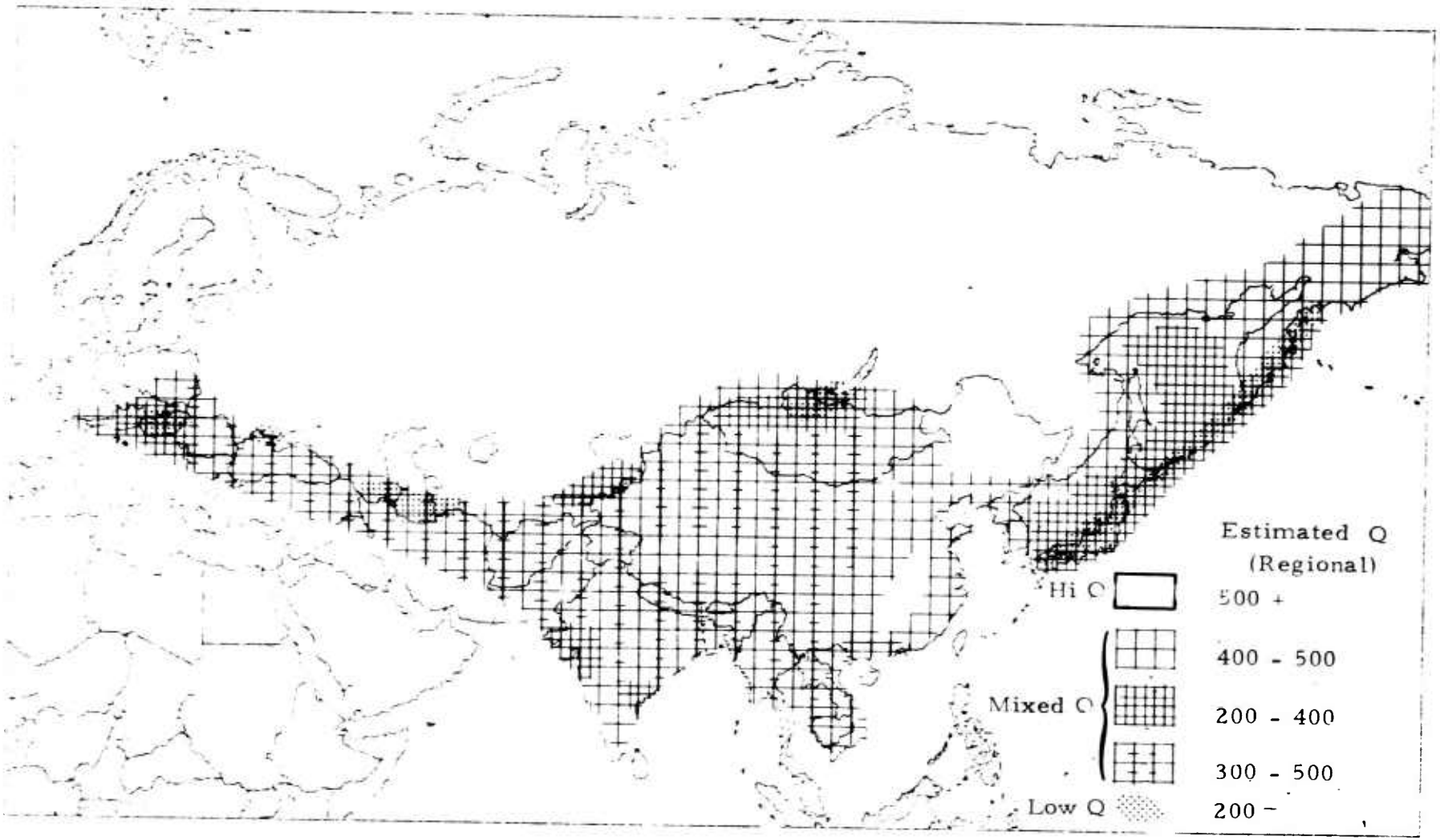

FIGURE II-5

ESTIMATED UPPER MANTLE Q FOR P-WAVES BENEATH EURASIA

SECTION III
REFERENCES

Alsup, S. A., 1973, Far Field Studies - Comparative Analysis of Upper Mantle Q and Other Geophysical Data on the Eurasian Continent, Semi-Annual Technical Report No. 1-Part A, Texas Instruments Report No. ALEX(02)-TR-73-01-Part A, AFOSR Contract No. F44620-73-C-0055, Texas Instruments Incorporated, Dallas, Texas.

Ben-Menahem, A., and D. G. Harkrider, 1964, Radiation Patterns of Seismic Surface Waves from Buried Dipolar Point Sources in a Flat Stratified Earth, J. Geophys. Res., 69, 2605.

Lane, S. S., 1973, Counterevasion Studies, Semi-Annual Technical Report No. 1-Part B, Texas Instruments Report No. ALEX(02)-TR-73-01-Part B, AFOSR Contract No. F44620-73-C-0055, Texas Instruments Incorporated, Dallas, Texas.

Lane, S. S., and D. Sun, 1974a, Counterevasion Studies, Semi-Annual Technical Report No. 2-Part B, Texas Instruments Report No. ALEX(02)-TR-74-01-Part B, AFOSR Contract No. F44620-73-C-0055, Texas Instruments Incorporated, Dallas, Texas.

Lane, S. S., and D. Sun, 1974b, Counterevasion Studies, Semi-Annual Technical Report No. 3-Part B, Texas Instruments Report No. ALEX(02)-TR-74-02-Part B, AFOSR Contract No. F44620-73-C-0055, Texas Instruments Incorporated, Dallas, Texas.

Lane, S. S., and D. Sun, 1975, Counterevasion Studies, Semi-Annual Technical Report No. 4-Part B, Texas Instruments Report No. ALEX(02)-TR-75-01-Part B, AFOSR Contract No. F44620-73-C-0055, Texas Instruments Incorporated, Dallas, Texas.

Schafer, R. W., 1969, Echo Removal by Discrete Generalized Linear Filtering, Technical Report 466, Research Laboratory of Electronics, M.I.T., Cambridge, Mass.

Schafer, R. W., and L. R. Rebiner, 1973, a Digital Signal Processing Approach to Interpolation, Proceedings of IEEE, vol 61, No. 6.

Sun, D., 1975, Counterevasion Studies, Semi-Annual Technical Report No. 5-Part B, Texas Instruments Report No. ALEX(02)-TR-75-02-Part B, AFOSR Contract No. F44620-73-C-0055, Texas Instruments Incorporated, Dallas, Texas.

Sun, D., 1976, Counterevasion Studies, Semi-Annual Technical Report No. 6-Part B, Texas Instruments Report No. ALEX(02)-TR-76-01-Part B, AFOSR Contract No. F44620-73-C-0055, Texas Instruments Incorporated, Dallas, Texas.

Tsai, Y. B., and K. Aki, 1970, Precise Focal Depth Determination from Amplitude Spectra of Surface Waves, J. Geophys. Res., 75, 5729.

Turnbull, L. S., 1976, Determination of Seismic Source Parameters Using Far-Field Surface Wave Spectra, Ph.D. Thesis, The Pennsylvania State University, University Park, Pennsylvania.

Turnbull, Jr., L. S., J. C. Battis, and David Sun, 1974a, Source Studies in the Near- and Far-Field, Semi-Annual Technical Report No. 3-Part A, Texas Instruments Report No. ALEX(02)-TR-74-03-Part A, AFOSR Contract No. F44620-73-C-0055, Texas Instruments Incorporated, Dallas, Texas.

Turnbull, Jr., L. S., J. C. Battis, David Sun, and A. C. Strauss, 1975a, Source Studies in the Near- and Far-Field, Semi-Annual Technical Report No. 4-Part A, Texas Instruments Report No. ALEX(02)-TR-75-01-Part A, AFOSR Contract No. F44620-73-C-0055, Texas Instruments Incorporated, Dallas, Texas.

Turnbull, Jr., L. S., David Sun, J. C. Battis, and F. Ringdal, 1975b, Source Studies in the Near- and Far-Field, Semi-Annual Technical Report No. 5-Part A, Texas Instruments Report No. ALEX(02)-TR-75-02-Part A, AFOSR Contract No. F44620-73-C-0055, Texas Instruments Incorporated, Dallas, Texas.

Turnbull, Jr., L. S., David Sun, and D. G. Black, 1974b, Determination of Seismic Source Parameters from Long-Period Teleseismic Waves, Semi-Annual Technical Report No. 2-Part A, Texas Instruments Report No. ALEX(02)-TR-74-01 -Part A, AFOSR Contract No. F44620-73-C-0055, Texas Instruments Incorporated, Dallas, Texas.

Turnbull, Jr., L. S., David Sun, and J. S. Shaub, 1973, Determination of Seismic Source Parameters from Frequency Dependent Rayleigh and Love Wave Radiation Patterns, Semi-Annual Technical Report No. 1-Part C, Texas Instruments Report No. ALEX(02)-TR-73-01-Part C, AFOSR Contract No. F44620-73-C-0055, Texas Instruments Incorporated, Dallas, Texas.